Granular Matter (2021) 23:21
https://doi.org/10.1007/s10035-021-01093-7

ORIGINAL PAPER

Wave transmission in 2D nonlinear granular-solid interfaces, including rotational and frictional effects

Chongan Wang[1] · **Qifan Zhang**[2] · **Alexander F. Vakakis**[1]

Received: 29 June 2020 / Accepted: 27 January 2021 / Published online: 9 March 2021

Abstract
We study the highly complex wave transmission at the interface between a two-dimensional (2D) hexagonally structured granular medium and a linearly elastic thin plate; we refer to this system as the "granular-solid interface". By applying an impulsive excitation at the free end of the granular medium we study the nonlinear acoustics at the interface. A computational model is developed, where the thin plate under the plane-stress assumption is discretized by finite-elements (FEs), whereas the granular medium by discrete-elements (DEs). Apart from the highly discontinuous Hertzian granule-to-granule and granule-to-plate interactions, we also take into account rotational and frictional effects in the granules; these effects render the acoustics of the granular-solid interface strongly nonlinear and highly discontinuous. The interaction forces coupling the granular medium to the plate are computed by means of an algorithm of interrelated iterations and interpolations at successive time steps. Since frictional effects may yield numerical instabilities, our approach incorporates the continuous "Coulomb–tanh" friction model, whose efficacy is verified through convergence studies. By formulating appropriate theoretically predicted convergence criteria, we show that the stability of the algorithm depends on the time step, the mesh size of the FE model, and the frictional model parameters. Accordingly, convergence is ensured by introducing a self-adaptive time step scheme, which is informed by theoretical convergence criteria. An application of the algorithm for a specific granular-solid interface demonstrates its validity, accuracy and robustness. Wave transmission through the discrete–continuum interface is drastically delayed by the granular medium, which, inflicts significant "softening" to the nonlinear acoustics. Moreover, there is strong nonlinear wave dispersion and energy localization in the granular medium, resulting in highly reduced wave transmission to the plate. Moreover, these nonlinear acoustical features are tunable with the applied shock (or input energy). The model and results presented in this work apply to a broad class of nonlinear discrete–continuum interfaces, with broad applications, e.g., shock/blast mitigation, granular containers with flexible boundaries and acoustic non-reciprocity.

Keywords Two dimensional granular-solid interface · Discrete element modelling · Nonlinear wave transmission · Ordered granular media

1 Introduction

Granular media composed of contacting discrete elastic particles (granules) has attracted considerable attention in the field of nonlinear acoustics from both practical and theoretical points of view. Nesterenko pioneered the study of pulse transmission in one-dimensional (1D) homogeneous granular chains composed of spherical, linearly elastic particles (granules) in Hertzian contact under zero or weak compression, and discovered the propagation of spatially localized, coherent, and shape-preserving, strongly nonlinear solitary pulses [1–4]. These so-called Nesterenko-solitary pulses result in intense momentum transfer through homogeneous granular chains and are tunable (self-adaptive) to energy or

✉ Qifan Zhang
hustzqf@gmail.com

✉ Alexander F. Vakakis
avakakis@illinois.edu

[1] Department of Mechanical Science and Engineering, University of Illinois at Urbana-Champaign, Urbana, IL 61801, USA

[2] School of Naval Architecture and Ocean Engineering, Huazhong University of Science and Technology, Wuhan 430074, China

pre-compression. Due to the governing nonlinear Hertzian interactions, the propagation speed of this class of solitary pulses exhibits strong dependence on the pulse amplitude, and is an order of magnitude slower than the speed of sound in the homogeneous elastic medium of the material of granules [4, 5]; hence, ordered granular media without pre-compression "slow' the propagation of waves, and, in fact, the linearized speed of sound (as defined in classical linear acoustics) in these media is zero, hence, their designation as "sonic vacua" by Nesterenko [1–4]. This means that their nonlinear acoustics is essentially nonlinear (i.e., devoid of any linearized components), while any weak pre-compression introduces a small linearized component in the acoustics and affects the speed of pulse transmission. In this work we will study exclusively 2D ordered sets of linearly elastic, spherical granules that are initially in contact with no pre-compression. Moreover, granular interactions will be strongly nonlinear due to Hertzian interactions during compression, "free flight" in the absence of compressive forces and ensuing collisions, and tangential frictional effects. We will model the collective dynamics of the considered granular assemblies by the discrete element (DE) method based on certain assumptions [6], which are satisfied in this work.

It is the strong tunability to (or, equivalently, passive self-adaptivity with) energy in synergy to the strong nonlinearity that yields interesting and unique nonlinear acoustic features in these media, having no counterparts in linear or weakly nonlinear acoustical systems. Indeed, it has been shown that the 1D ordered granular media can support tunable (with energy) frequency pass bands [7], traveling waves [8], intense nonlinear energy exchanges [9], targeted energy transfers [10], and even break of acoustic reciprocity [11–13]. Inspired by these distinctive acoustical features of granular media, previous studies exploited these unique characteristics and reported various potential engineering applications such as shock mitigation and energy absorbing layers [14–16], acoustic imaging devices [17], nonlinear acoustic lenses [18, 19], passive acoustic filters [20] and acoustic switches [21].

To incorporate the remarkably versatile nonlinear acoustics of ordered granular media into practical applications, a natural step is to try to gain a better physical insight and understanding on the complex interactions of these highly discontinuous media with linearly elastic homogenous continua at their boundaries. Typical boundary conditions that were considered in studies of granular media were the standard ones, namely, traction-free or fixed boundaries [22], and only a limited number of works considered the effects of "non-standard" flexible boundaries. The reflection and localization of solitary waves propagating in the 1D granular chains and interfacing with a cylindrical elastic medium [23] or thin plate [24] have been previously explored. It was found that the formation and propagation of reflected solitary waves from the flexible interface was significantly influenced by the bounding medium's mechanical properties, such as the elastic modulus, thickness and geometry, as well as the size of the granules. Potekin et al. [25] developed an iterative numerical algorithm to study nonlinear wave scattering at the interface of 1D dimer granular chains with an elastically supported linear elastic string, while Zhang et al. [26] extended the numerical algorithm to study the nonlinear acoustics of a 1D granular chain interfacing with a membrane. Both investigations showed that the energy eventually transferred from the granular chain to the flexible boundary was inversely proportional to the local stiffness at the interface.

Nonlinear wave propagation in 2D and 3D granular media has been largely unexplored with only a limited number of recent works appearing in the literature on force chains, and ordered or disordered lattices [27–42]. Perhaps this is due to the complex nature of granular interactions in two dimensions, which involve axial as well as tangential loads. Amnaya et al. [27] and Li et al. [43] numerically investigated impulse-induced wave propagation in closely packed 2D granular media, observing the propagation of 2D solitary waves. Likewise, Leonard [30] reported on decaying propagating pulses in 2D hexagonal granular assemblies. Moreover, intense nonlinear energy exchanges in coupled 2D granular networks were studied by reduced order models, capturing interesting nonlinear dynamical phenomena. These include *nonlinear energy equi-partition* [34, 44, 45] and *beat phenomena* [46]; nonlinear targeted energy transfers [10]; and other interesting response regimes [47, 48]. Leonard and Daraio [28] studied the capacity of 2D granular crystals to alter the shape of propagating wavefronts in 2D ordered granular arrays, whereas Leonard et al. [29] examined the rapid reduction of the amplitudes of primary pulses traveling through networks of interconnected chains of particles. Lisyansky et al. [35] provided analytical approximations for primary wave transmission in hexagonally packed and damped granular crystals with a spatially varying cross section using a nonlinear mapping technique and homogenization.

Typically, 2D numerical models account only for axial Hertzian interactions between granules and neglect dissipation effects, particularly those related to relative rotations between granules yielding frictional effects. Yet neglecting such effects may lead to significant modeling errors and deviations of the computational predictions from experimental measurements. This was clearly demonstrated by Yang and Sutton [49] who studied the propagation of nonlinear waves in a hexagonally packed granular channel and proved that the rotational dynamics of the granules influence significantly the dynamics. Moreover, Goldenberg and Goldhirsch [50], Chattoraj et al. [51] and Charan et al. [52], showed that frictional forces play an important role in the

dynamics of 2D granular media, even leading in some cases to dynamical instabilities. Hence, accounting for rotational and frictional effects in 2D ordered granular configurations can significantly improve the agreement between simulations and experiments [12, 50]. Furthermore, to the best of the authors' knowledge there is no rigorous prior work on the interaction of 2D (or 3D) granular media with flexible boundaries. Such a multi-dimensional interaction between a strongly nonlinear 2D granular medium and a linearly elastic (receiving) medium poses distinct challenges, given the highly discontinuous, strongly nonlinear and transient nature of the granule-medium interactions, as well as the complexity stemming from the dispersive wave dynamics in both media. Moreover, rotational frictional effects in the granule-to-granule and granule-to-flexible boundary interactions further complicates the computational modeling.

The main aim of the present work is to formulate a computationally efficient and robust computational algorithm to model the strongly nonlinear acoustics of interfaces between 2D ordered granular media and linearly elastic plates; we will refer to these discrete–continuous systems as "granular-solid interfaces". In this work the acoustics of the thin plate will be modeled by the finite element (FE) method based on the simplifying plane-stress assumption. In addition, the 2D planar motions of the granular medium (assuming that it is without any pre-compression) will be modeled by the discrete element (DE) method. Our approach will take full account of compressive Hertzian granule-to-granule and granule-to-plate interactions, as well as, of relative granule rotations yielding frictional effects. Hence, there will be *three major sources of strong nonlinearity in the 2D granular media under consideration, namely, Hertzian contacts, "free flights" of granules followed by collisions between them or with the plate boundary, and frictional tangential interactions*. As a result, the acoustics of the wave transmission and scattering through the granular-solid interface is expected to be highly discontinuous, nonlinear and complex. Apart from developing the computational algorithm discussed herein, we wish to provide an example with a specific granular-solid interface that will validate the algorithm and demonstrate its accuracy and robustness. Moreover, the example will highlight the capacity of the granular medium to drastically "slow down" the transmitted stress wave front and drastically disperse it before it transmits to the thin plate.

The contents of the paper are structured as follows. In Sect. 2, we introduce the model for the granular-plate interface. Then in Sect. 3, the iterative/interpolative computational algorithm based on a combined FE/DE analysis is discussed, and convergence criteria are theoretically derived to ensure robustness of the computation. An example of application is presented in Sect. 4 to illustrate the efficacy and accuracy of the computational algorithm and highlight the capacity of the granular-solid interface to drastically attenuate transmitted stress waves; to this end, comparison of the acoustics of the interface to a "monolithic" plate system is made. Finally, in Sect. 5 we summarize the main results and discuss some possible future research directions.

2 Model of the granular-solid interface

We consider wave transmission in the 2D granular-solid interface shown in Fig. 1. The elastic solid medium is a linearly elastic thin plate, whereas the granular interface is an ordered network of granules with no prior compression. A distributed shock (impulse) excitation is applied at the left boundary granules of the granular medium at a direction normal to the edge of the contacting plate (cf. Fig. 1), while, apart from the boundary in contact with the granular medium, the other boundaries of the thin plate are assumed to be either clamped or traction-free. Moreover, before the application of the impulsive excitation the system is in a state of rest. As a simplifying assumption we will assume that all deformations, rotations and forces are planar. The granules interact with each other and with the boundary of the plate though axial (Hertzian) and tangential (frictional) forces, so there is direct coupling between the granular medium and the thin plate. We are interested on the *early-time (primary) wave front transmission* through the granular-solid interface, especially before secondary wave reflections at the plate boundaries occur. Following previous works [25, 26] we will apply the discrete element (DE) method to model the granular medium, and the finite element (FE) method to model the elastic plate. Special attention will be given to the accurate modeling of the compatibility of deformations, rotations and forces at the boundary between the granular medium and the thin plate, as well as the overall energy conservation that includes dissipative effects.

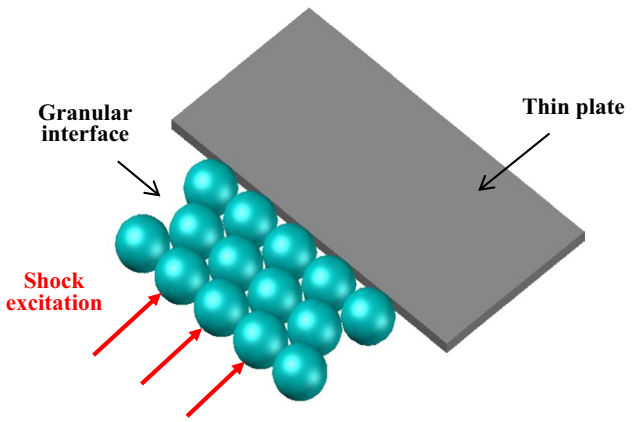

Fig. 1 Schematic of the granular-solid interface subject to shock excitation

2.1 Discrete element (DE) modeling of the 2D granular medium

Considering the initially uncompressed 2D hexagonal granular medium of Fig. 1, we assume that it is composed of a number of identical and spherical granules that are in point contact with each other prior the application of the applied excitation. The granules themselves are linearly elastic. However, the granular system is strongly nonlinear due to the granule-granule and granule-plate contact interactions. Following the application of the shock excitation, and under certain assumptions related to small elastic deformations [6], the nonlinear planar dynamics of the granules are simulated using the discrete element (DE) method that approximates each granule as a point mass [6, 53, 54] with three degrees of freedom, i.e. two translational degrees of freedom and one rotational degree of freedom (cf. Fig. 2). There are three sources of nonlinearity in this system, namely (i) Hertzian interactions under compressive loads, (ii) collisions between granules after separation and "free flight," and (iii) frictional forces due to granule rotations; moreover, such nonlinear interactions occur not only between neighboring granules in the interior of the granular medium, but also between granules that are in contact with the boundary of the thin elastic plate. All these nonlinearities will be accounted in the DE simulation, by constructing a new 2D granular interaction model based on a prior model developed by Yang and Sutton in [49], and optimally incorporating (important) frictional model. Indeed, as discussed in [49], omitting rotational and frictional effects in 2D granular networks leads to erroneous results (see also [12]).

In the DE model the kinematic equations of motion of a single granule are given by (where unless otherwise noted bold symbols denote (2×1) vectors),

$$\ddot{\boldsymbol{s}}_i = \frac{\sum_j (\boldsymbol{N}_{ij}+\boldsymbol{f}_{ij})+\sum_k (\boldsymbol{N}_{ik}+\boldsymbol{f}_{ik})}{m_i}; \quad \ddot{\boldsymbol{\theta}}_i = \frac{R_i \sum_j (\boldsymbol{n}_{ij}\times\boldsymbol{f}_{ij})+R_i \sum_k (\boldsymbol{n}_{ik}\times\boldsymbol{f}_{ik})}{I_i} \tag{1}$$

where $\boldsymbol{s}_i$ denotes the displacement vector and $\boldsymbol{\theta}_i = \theta_i \boldsymbol{k}$ the angular displacement pseudo-vector for the ith granule—where θ_i denotes the amplitude of $\boldsymbol{\theta}_i$ and $\boldsymbol{k}$ denotes the unit pseudo-vector assuming positive anti-clockwise rotation, R_i denotes the radius of ith granule, and overdot denotes differentiation with respect to the time variable τ. In (1) m_i denotes the mass and I_i the moment of inertia of the ith granule, respectively, where for spherical granules, $I_i = (2/5)m_i R_i^2$. Referring to Fig. 2, the vectors $\boldsymbol{N}_{ij}$ and $\boldsymbol{f}_{ij}$ denote the normal and tangential (friction) force acting on the ith granule by the jth granule respectively, whereas, $\boldsymbol{N}_{ik}$ and $\boldsymbol{f}_{ik}$ denote the normal and friction force acting on the ith granule by the thin plate at the boundary, respectively. The vector $\boldsymbol{n}_{ij}$ is the position vector pointing from the center of ith granule to the center of jth granule, and is defined as $\boldsymbol{n}_{ij} = (\boldsymbol{s}_j - \boldsymbol{s}_i)/\left(\left|\boldsymbol{s}_j - \boldsymbol{s}_i\right|\right)$. Similarly, $\boldsymbol{n}_{ik}$ is the vector pointing from the center of the ith boundary granule perpendicular to the point k on the boundary of the thin plate (cf. Fig. 2); note that the contact point k on the boundary is located on a granule–specific point which "moves" with its neighboring contacting granule so that the unit vector $\boldsymbol{n}_{ik}$ is always normal to the boundary of the thin plate.

In the DE model the kinematic Eqs. (1) need to be supplemented by a set of constitutive equations. To this end, the normal force $\boldsymbol{N}_{ij}$ between two interacting granules under compression obeys the following Hertzian law [49, 53, 54],

$$\boldsymbol{N}_{ij} = -\left(A_{ij}\delta_{n,ij}^{3/2} + \gamma_{ij}\dot{\delta}_{n,ij}\right)\boldsymbol{n}_{ij} \tag{2}$$

where $\delta_{n,ij}$ denotes the radial relative deformation (overlap) between the geometric centers of the two interacting granules i and j, defined as $\delta_{n,ij} = max\left(R_i + R_j - \left|\boldsymbol{s}_j - \boldsymbol{s}_i\right|, 0\right)$, indicating that expression (2) is valid only when the argument in the parenthesis is non-zero when $\delta_{n,ij} > 0$ while it is zero otherwise; this models the absence of interaction between granules in the absence of compression between them. The scalar constants A_{ij} and γ_{ij} are the elastic and viscous damping coefficients in the normal contact force between granules, respectively, and depend on the material and geometric parameters of the granules, as well as the relative deformation $\delta_{n,ij}$,

$$A_{ij} = (4/3)E^*\sqrt{R^*}, \quad \gamma_{ij} = \alpha_n\left(m^* A_{ij}\right)^{1/2}\delta_{n,ij}^{1/4} \tag{3}$$

where α_n is a constant coefficient related to the restitution coefficient of the granules [53], E^* denotes the effective Young's modulus, R^* the effective radius and m^* the effective mass defined as:

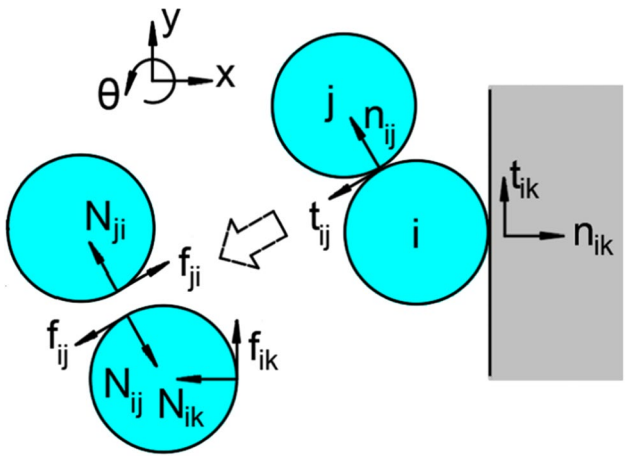

Fig. 2 Free body diagram for granule–granule and granule–thin plate interactions, showing normal and tangential unit vectors and forces

$$\frac{1}{E^*} = \frac{1-\nu_i^2}{E_i} + \frac{1-\nu_j^2}{E_j}; \frac{1}{R^*} = \frac{1}{R_i} + \frac{1}{R_j}; \frac{1}{m^*} = \frac{1}{m_i} + \frac{1}{m_j} \tag{4}$$

In (4) $E_{i(j)}$, $R_{i(j)}$, $m_{i(j)}$ and $\nu_{i(j)}$ denote the Young's modulus, radius, mass and Poisson ratio of the ith(jth) granule. The Hertzian model (2) also applies to model the contact between the boundary granule and the thin plate by replacing the normal relative deformation $\delta_{n,ij}$ by the relative normal deformation $\delta_{n,ik}$ between the center of the granule and the thin plate. In this case the coefficients A_{ik} and γ_{ik} are defined similarly to Eq. (3) with $E^* = \frac{E_i}{1-\nu_i^2}$, $m^* = m_i$, and $R^* \to R_i$ given that the flat boundary of the thin plane has infinite radius of curvature. The model (2) is reliable for the collision of two granules in free flight. In this work, we study exclusively closely-packed granules. Hence, we will employ model (2) for the following computational work (following previous works [12, 49]), taking into account that the estimation of the dissipation is approximate, but still valid for studying the nonlinear acoustics.

Considering now the tangential force component on a granule, if its magnitude is much smaller than the corresponding normal force, the previous Hertzian model is still applicable for approximating the normal force [6]. Under this assumption, the tangential deformations of the granules are neglected [49] (this is within the assumptions of the DE modeling of the granular dynamics [6]), and we only consider the slide frictional force in the tangential direction on the granule surfaces. For reasons related to numerical stability of the DE simulations, in our work, a continuous smooth Coulomb-tanh model [55, 56] is adopted in order to ensure convergence of the numerical results. Accordingly, the frictional forces applied to the granules due to their rotations are approximated as (cf. Fig. 2),

$$\boldsymbol{f}_{ij} = -\mu \left| N_{ij} \right| \tanh\left(k_s \dot{\delta}_{t,ij}\right) \boldsymbol{t}_{ij} \tag{5}$$

where μ is the friction coefficient (assumed to be constant), k_s is a parameter controlling the smoothness of the frictional law, and $\dot{\delta}_{t,ij}$ denotes the (scalar) tangential relative velocity between granules at the contact point:

$$\dot{\delta}_{t,ij} = \left[\left(\dot{\boldsymbol{s}}_i + R_i \dot{\boldsymbol{\theta}}_i \times \boldsymbol{n}_{ij}\right) - \left(\dot{\boldsymbol{s}}_j + R_j \dot{\boldsymbol{\theta}}_j \times \boldsymbol{n}_{ji}\right)\right] \cdot \boldsymbol{t}_{ij} \tag{6}$$

In (6) $\boldsymbol{t}_{ij}$ denotes the unit vector in the tangential direction of the contact interface between the ith and jth granules. The unit vector $\boldsymbol{t}_{ij}$ is perpendicular to the normal unit vector $\boldsymbol{n}_{ij}$ and the positive direction of $\boldsymbol{t}_{ij}$ is defined such that $\boldsymbol{t}_{ij} = \boldsymbol{k} \times \boldsymbol{n}_{ij}$ (cf. Fig. 2). Clearly, the friction model (5) is also applicable for the tangential force $\boldsymbol{f}_{ik}$ between a boundary granule and the thin plate (cf. Fig. 2) if we replace the relative tangential velocity between granules, $\dot{\delta}_{t,ij}$, with the relative tangential velocity $\dot{\delta}_{t,ik}$ between the contact granule and the plate.

At this point we make some remarks regarding the frictional coefficient in the Coulomb-tanh model (5). In particular, it can be shown that for relatively large tangential relative velocity $\left|\dot{\delta}_{t,ij}\right|$ and/or large coefficient k_s, so that $k_s \left|\dot{\delta}_{t,ij}\right| \gg 1$, the Coulomb-tanh model approaches the classical Coulomb friction model; whereas if $k_s \left|\dot{\delta}_{t,ij}\right| \ll 1$, the Coulomb-tanh model approaches the classical viscous damping model. We note that as k_s increases the visco-elastic effect in the Coulomb-tanh model also increases, but disproportionally compared to the overall dissipative effect of the model; hence, in that case the visco-elastic effect can be neglected compared to the nonlinear friction component. As discussed in a later Section, the appropriate choice of the coefficient k_s plays an important role for correctly accounting of the frictional effects, and the numerical stability of the numerical DE simulations.

Another way to verify the accuracy of the following numerical simulations is physics-based, namely, by checking the conservation of instantaneous total energy in the entire granular-solid interface. Indeed, given that the initial energy that is induced to the granular medium by the applied impulsive loads can be accurately estimated, one can verify that at each time instant of the simulation the summation of the potential and kinetic energies of the granular medium and the plate, as well as the total dissipated energy up to that time instant, are conserved. Considering the DE simulations of the granular medium, the instantaneous potential and kinetic energy of each granule can be directly estimated. For simplicity, the potential energy due to granule-granule elastic interaction is equally assigned between the interacting granules, whereas the potential energy due to granule-thin plate interaction is fully assigned to the granule. Therefore, the instantaneous energy of each granule of the granular medium is expressed as follows,

$$E_{bi}(t) = \frac{1}{2} m_i \left|\dot{\boldsymbol{s}}_i(t)\right|^2 + \frac{1}{2} I_i \dot{\theta}_i^2(t) + \sum_j (1/5) A_{ij} \delta_{n,ij}^{5/2}(t) + \sum_k (2/5) A_{ik} \delta_{n,ik}^{5/2}(t) \tag{7a}$$

$$GI(t) = \sum_i E_{bi}(t) \tag{7b}$$

where $E_{bi}(t)$ denotes the total instantaneous (kinetic and potential) energy on the ith granule and $GI(t)$ the total instantaneous energy of the granular medium.

Moreover, since the granular medium is dissipative due to structural (viscous) damping in the interior of the granules and frictional interactions, the total energy $D(t)$ dissipated up to time instant t is computed based on the work performed by the dissipative forces,

$$W_{\text{friction}}(t) = \int_0^t \left[\sum_i \left(\sum_j \boldsymbol{f}_{ij}(\tau) \cdot \left(\dot{\boldsymbol{s}}_i(\tau) + R_i \dot{\theta}_i(\tau) \boldsymbol{t}_{ij} \right) + \sum_k \boldsymbol{f}_{ik}(\tau) \cdot \left(\dot{\boldsymbol{s}}_i(\tau) + R_i \dot{\theta}_i(\tau) \boldsymbol{t}_{ik} \right) \right) \right] d\tau \leq 0 \tag{8a}$$

$$W_{\text{viscous}}(t) = \int_0^t \left[\sum_i \left(\sum_j \gamma_{ij} \dot{\delta}_{n,ij}(\tau) \boldsymbol{n}_{ij} \cdot \dot{\boldsymbol{s}}_i(\tau) + \sum_k \gamma_{ik} \dot{\delta}_{n,ik}(\tau) \boldsymbol{n}_{ik} \cdot \dot{\boldsymbol{s}}_i(\tau) \right) \right] d\tau \leq 0 \tag{8b}$$

$$D(t) = -\left[W_{\text{viscous}}(t) + W_{\text{friction}}(t) \right] \geq 0 \tag{8c}$$

where $W_{\text{friction}}(t)$ and $W_{\text{viscous}}(t)$ denote the work performed by the frictional and internal viscous forces up to time instant t, respectively. Note that since the work performed by the dissipative forces always non-positive, the total dissipated energy being the negative of this work is non-negative at each time instant. The total energy of the granular medium including the dissipated energy is given by the expressions (7) and (8). The total instantaneous energy of the granular-solid interface is conserved, taking into account the expressions (7) and (8) together with the instantaneous energy of the plate. The conservation relation will be evaluated at each time instant of the following numerical simulations as a check of the accuracy of the computational results.

2.2 Finite element (FE) modeling of the thin plate under the plane stress assumption

The plate is assumed to be planar, orthogonal and with small thickness in the dimension normal to the plane. The thin plate is assumed to have three clamped or traction-free edges, while the fourth traction-free edge is in contact with the boundary granules and constitutes the granular-solid interface. Under these conditions the plane stress model is applied so that the full 3D infinitesimal elasticity equations of the plate are simplified to a 2D model that is compatible with the corresponding 2D DE model of the granular medium. The plane stress approximation has been shown to be valid in the limit of small thickness of the plane or curved plates [57]. To this end, we start by considering the full 3D infinitesimal elasticity equations in the interior continuum of the plate [58],

$$\rho \ddot{\boldsymbol{u}} - \nabla \cdot \boldsymbol{\sigma} = 0 \tag{9a}$$

$$\boldsymbol{\varepsilon} = (1/2)\left[\nabla \boldsymbol{u} + (\nabla \boldsymbol{u})^T \right] \tag{9b}$$

$$\boldsymbol{\sigma} = \boldsymbol{E}\boldsymbol{\varepsilon} \tag{9c}$$

where $\boldsymbol{\sigma}$ denotes the stress tensor, $\boldsymbol{\varepsilon}$ the strain tensor, $\boldsymbol{E}$ the elastic (stiffness) tensor, $\boldsymbol{u}$ the displacement vector and ρ the density of the material of the plate. In addition, ∇ represents the nabla symbol and $(\cdot)^T$ the transpose operator. Assuming that the thin plate is composed of a metal, it is appropriate to assume that it has small capacity for internal (structural) dissipation. Notice that in the granular system, we applied the DE model where we implicitly assumed that the wave transmission in the granular medium is much slower than the wave transmission within each granule (i.e., in the bulk). Moreover, we assume that the dissipative effect mainly originates due to granular interactions, where we infer that the dissipative effect in the elastic solid (plate) is much smaller compared to the dissipative effect in the granular medium, so the internal (structural) dissipation in the plate may be neglected altogether. This is justified even further, when we note that the (linear) acoustics in the plate is much faster than the (nonlinear) acoustics in the granular medium (this is verified computationally later in this work), that the structural loss factor of steel is very low, and, lastly, since we are only interested in the *early-time wave transmission* through the thin plate, when the effects of structural (internal) dissipation are expected to be minimal due to the relatively fast speed of the wave front. This is not so in the granular medium where primary pulse transmission will be shown to be considerably slower, nonlinear and non-smooth so that dissipative effects are stronger compared to the plate and need to be accounted for—see discussion that follows.

Imposing the plane-stress assumption we assume that the out-of-plane stress components in the z-direction are zero, $\sigma_z = \sigma_{xz} = \sigma_{yz} = 0$, the reduced 2D stress–strain equations for equilibrium and compatibility are given by,

$$\rho\left(\ddot{u}_x, \ddot{u}_y\right)^T = \left(\frac{\partial \sigma_x}{\partial x} + \frac{\partial \sigma_{xy}}{\partial y}, \frac{\partial \sigma_{xy}}{\partial x} + \frac{\partial \sigma_y}{\partial y}\right)^T \tag{10a}$$

$$\left(\varepsilon_x, \varepsilon_y, \gamma_{xy}\right)^T = \left(\frac{\partial u_x}{\partial x}, \frac{\partial u_y}{\partial x}, \frac{\partial u_x}{\partial y} + \frac{\partial u_y}{\partial x}\right)^T \tag{10b}$$

$$\left(\sigma_x, \sigma_y, \sigma_{xy}\right)^T = \frac{E}{1-\nu^2}\begin{pmatrix} 1 & \nu & 0 \\ \nu & 1 & 0 \\ 0 & 0 & (1-\nu)/2 \end{pmatrix}\left(\varepsilon_x, \varepsilon_y, \gamma_{xy}\right)^T \tag{10c}$$

where u_x and u_y denote the displacements in the x and y directions, respectively, $\varepsilon_x, \varepsilon_y$ and γ_{xy} the normal and shear strains, whereas σ_x, σ_y and σ_{xy} the normal and shear stresses in the plane; in addition, E and ν denote the Young's modulus and Poisson's ratio of the material, respectively. These equations are discretized in the following FE simulations.

We note that in the plane-stress assumption the deformation along the thickness is approximately uniform. However, the plane stress assumption is not expected to hold at the granular-solid interface since the contact area between a boundary granule and the plate is expected to be approximately circular under compression. To overcome this inconsistency, we assume that there are small rigid layers that are perfectly bonded on the plate at each granule-plate interface, as shown in Fig. 3 [59]. These layers are assumed to be perfectly rigid, and with negligibly small thickness and mass; moreover, the total length of each rigid layer should be much smaller than a characteristic length of the granule-solid interface so that its effect on the dynamics of the plate is small.

Typically, for ordered granular media with identical close-packed granules, the length of each rigid layer should be much smaller than the radius of the granule (which represents the previous characteristic length). Then, St. Venant's principle [57] ensures that the rigid layers do not have any significant effects on the response in the far field of the solid medium. Note that only rigid body motions are allowed for the rigid layers, and as they are approximately massless, the forces applied on the rigid layer by the contacting granule and the supporting plate are in equilibrium. As an approximation, we assume that the contact force by the granule is applied at the middle of the rigid layer, and that the directions of the normal and tangential forces on the later are invariant. These assumptions are legitimate provided that the deformations in the granular-plate system are small. Under these conditions, the rigid layers transmit directly compressive forces from the boundary granules to the plate without violating the overall plane-stress approximation. Moreover, the normal and tangential forces exerted by the granules to the rigid layers can be computed as discussed previously; these forces are transmitted through the rigid layers directly to the plate.

The finite element (FE) method was applied to discretize the 2D plane-stress equations of motion (9a) subject to the approximate constitutive Eq. (10c). In this work, 8-node quadrilateral isoparametric elements [60, 61] are employed for the discretization of the elastic continuum. Moreover, special care is given on the FE modeling of the rigid layers that connect the contacting granules to the thin plate. To this end, we impose multi-point constraints on the nodes of the FE mesh on each rigid layer, so that the translational and tangential degrees of freedom (x- and y-directions, respectively in Fig. 3) of the center node of each rigid layer as a whole are considered as the *driving* degrees of freedom, whereas the other nodes of the rigid layer are considered as *driven*; this can be performed by formulating a transformation matrix and reducing the driven degrees of freedom. The modified result of FE modeling is the following discretization of the thin plate with the attached rigid layers,

$$\boldsymbol{M}\ddot{\boldsymbol{x}} + \boldsymbol{K}\boldsymbol{x} = \boldsymbol{F} \tag{11}$$

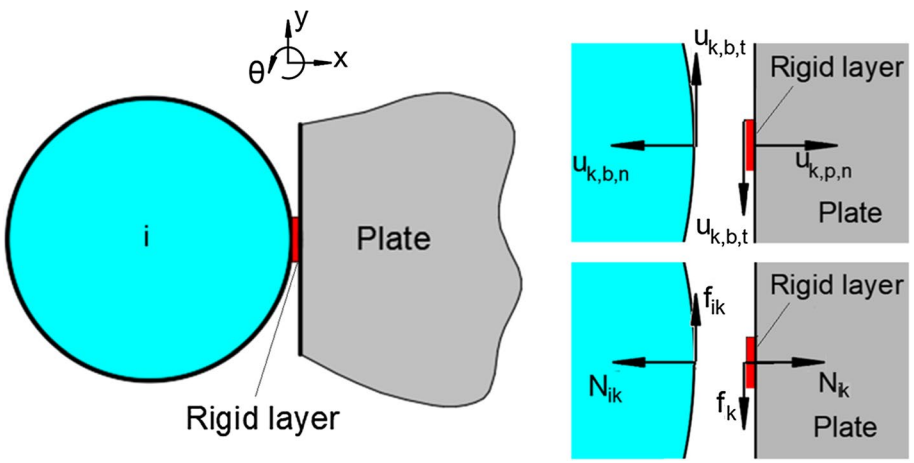

Fig. 3 Schematic diagram of the contact interaction model between a boundary granule and the thin plate through the rigid layer, with interaction forces and displacements at the boundary shown (positive directions are indicated); note the notation for the normal and tangential interaction forces applied to k-th node of the plate, $N_k \equiv N_{ik}$ and $f_k \equiv f_{ik}$, respectively

where $\boldsymbol{x}$ denotes the displacement vector involving the generalized displacements of all nodes, $\boldsymbol{M}$ the system mass matrix of the plate, $\boldsymbol{K}$ the corresponding system stiffness matrix, $\boldsymbol{F}$ the force vector applied to the plate, and overdot the differentiation with respect to the time variable τ. It is worth mentioning that the elements related to the driving degrees of freedom (DOFs) in $\boldsymbol{F}$ are the corresponding coupling interaction forces applied to the rigid layers by the granular medium with which it couples, and the other elements remain zero.

Furthermore, in correspondence to the previous energy measures that were formulated the granular medium, we introduce the following energy measures for the thin plate,

$$E^e = \frac{1}{2}(\boldsymbol{x^e})^T \boldsymbol{K}^e(\boldsymbol{x^e}) + \frac{1}{2}(\dot{\boldsymbol{x}}^e)^T \boldsymbol{M}^e(\dot{x}^e) \tag{12a}$$

$$PE = \sum_{\text{Elements}} E^e = \frac{1}{2}\boldsymbol{x}^T \boldsymbol{K}\boldsymbol{x} + \frac{1}{2}\dot{\boldsymbol{x}}^T \boldsymbol{M}\dot{\boldsymbol{x}} \tag{12b}$$

where E^e denotes the instantaneous energy of each finite element, $\boldsymbol{x^e}$ the element displacement vector, $\boldsymbol{K}^e$ and $\boldsymbol{M}^e$ the element stiffness and mass matrices, respectively, and PE the total instantaneous (kinetic and elastic) energy of the plate. The conservation law is given by $GI(t) + D(t) + PE(t) = E$, where E is the initial energy induced to the system by the shock excitations. The energy measures of the plate given by (12), together with the corresponding measures (7) and (8) for the granular medium, will enable the detailed investigation of complex, nonlinear energy transmission and reflection at the interface between the granular medium and the thin plate.

In synopsis, the integrated granular-solid system is governed by the nonlinear Eq. (1) and the linear Eq. (11), which are coupled through the coupling force vector $\boldsymbol{F}$ applied to the plate through the rigid layers. Clearly this vector cannot be evaluated in closed form since it is determined by the solution itself, i.e., by the transient record of the highly nonlinear and discontinuous (non-smooth) interactions between the boundary granules and the free edge of the plate. The accurate and robust numerical computation of this transient force vector requires special consideration and is the main focus of this work; this is discussed in detail in the next Section where the computational algorithm is discussed in detail. By solving the coupled equations of motion, we can study the complex, early-time nonlinear wave scattering that occurs at the granular-solid interface and characterize the (energy dependent) transmission and reflection features of the governing nonlinear acoustics. To the authors' best knowledge this is the first such computation reported in the literature.

3 Computational algorithm

A computational algorithm was developed to model the complex acoustics of the granular-solid interface by numerically solving the strongly nonlinear DE Eq. (1) for the granular medium concurrently to the linear FE Eq. (11) for the thin plate. These two sets of equations are coupled through the interaction forces at the 2D interface, which need to be solved accurately and robustly. A similar (in spirit) algorithm was developed in two previous works [25, 26], but for much simpler, 1D granular media (where friction effects do not need to be accounted for) interacting with flexible systems (chords or membranes). Special consideration is given to the numerical stability of the algorithm, in view of the frictional effects in the granular medium which may lead to instabilities [50–52].

Given the great disparity between the DOFs of the linear FE Eqs (11) and the nonlinear DE Eq. (1) (as there are much more many degrees of freedom in the FE plate model), it is necessary to solve Eqs (11) and (1) separately. Moreover, it is critical to accurately compute the highly discontinuous, nonlinear interaction forces that couple the FE and DE models; as highlighted in Fig. 3, these forces represent normal (Hertzian) and tangential (frictional) contact forces between the boundary granules and the free edge of the thin plate. In this work, we will compute the interaction forces through a robust iterative computational algorithm, whose origin can be traced in [25, 26], but for much simpler, 1D granular media interacting with flexible systems (chords or membranes) at their boundaries. Here we provide a brief synopsis of the basic elements of the algorithm, and for a more detailed exposition we refer to "Appendix 1".

The computational algorithm is outlined in the flow chart of Fig. 13 in "Appendix 1". The coupled granular-solid system viewed as an integrated acoustical system is discretized into time steps. *Central to the algorithm is the accurate computation of the complex, highly discontinuous and strongly nonlinear interaction forces between the granular medium and the plate*. In terms of notation, the subscript s ($s+1$) denotes a vector evaluated at the time instant τ_s (τ_{s+1}), where the time step is given by $\Delta\tau = \tau_{s+1} - \tau_s$. The force vector applied to the plate in (11) at the time instant τ_{s+1} is denoted by $\boldsymbol{F}_{s+1}$, containing all interaction forces. The only non-zero terms in the global force vector $\boldsymbol{F}_{s+1}$ are located at the normal and tangential driving DOFs; for simplicity these are partitioned in terms of the normal force vector $\boldsymbol{N}_{s+1}$ and the tangential force vector $\boldsymbol{f}_{s+1}$ at the given time instant τ_{s+1}, so $\boldsymbol{F}_{s+1} \equiv (\boldsymbol{N}_{s+1}, \boldsymbol{f}_{s+1})$. Specifically, the k-th elements in the force vectors $\boldsymbol{N}_{s+1}$ and $\boldsymbol{f}_{s+1}$ are the components at the normal and tangential DOFs of the node at the k-th contact point,

that is, the normal and tangential forces, $N_{k,s+1}$ and $f_{k,s+1}$, respectively, applied at the k-th contact point (node) on the plate at the time instant τ_{s+1} (cf. Fig. 3). As discussed below an iterative method is employed to compute the force vectors $\boldsymbol{N}_{s+1}$ and $\boldsymbol{f}_{s+1}$, with initial guesses (at iteration $j = 1$) chosen as $\boldsymbol{N}_{s+1}^{(1)} = \boldsymbol{N}_s^C$ and $\boldsymbol{f}_{s+1}^{(1)} = \boldsymbol{f}_s^C$. Here the superscript C denotes convergence, so $\boldsymbol{N}_s^C$ and f_s^C are the converged normal and tangential interaction forces at the previous time instant τ_s, respectively; furthermore, the order of the iteration is denoted by the superscript in parenthesis.

The iteration scheme is performed in two phases. In the first phase we consider exclusively the response of the thin plate. To demonstrate the iterative scheme, we start with the first iteration ($j = 1$) in the flow chart of Fig. 13 ("Appendix 1") at the time instant τ_{s+1}. The first estimate for the force vector applied to the plate is taken as $\boldsymbol{F}_{s+1}^{(1)} = \boldsymbol{F}_s^C$, as discussed previously Then, the first iteration of the response of the plate, $\boldsymbol{x}_{s+1}^{(1)}$, at the same time instant τ_{s+1} is computed by solving Eq. (11) using the β-Newmark method under on the assumption of constant acceleration between successive time steps (see "Appendix 1"). Then interpolation is used to compute the first iteration of the plate response in the entire interval $\tau \in [\tau_s, \tau_{s+1}]$. This also computes the responses of the rigid layers at the interface, which act, in essence, as moving boundaries for the DE system governing the granular medium. This completes the first phase of the first iteration for the plate response. In the second phase of the first iteration (i.e., still with $j = 1$), we compute the response of the granular medium by solving numerically the DE Eqs (1) of the granular medium in the time interval $\tau \in [\tau_s, \tau_{s+1}]$. This is performed using the fourth order Runge–Kutta method (see details in "Appendix 1"). Hence, *in the second phase of the first iteration, the response of the granular medium is computed for* $\tau \in [\tau_s, \tau_{s+1}]$ *by "relaxing" the positions of the contact points with the plate; this, in turn, informs the updated interaction force vector applied to the plate*. This yields the second iteration for the interaction forces, $\boldsymbol{F}_{s+1}^{(2)} \equiv \left(\boldsymbol{N}_{s+1}^{(2)}, \boldsymbol{f}_{s+1}^{(2)}\right)$, at the time instant τ_{s+1} by applying Eqs (2) and (5) with the first iteration responses of the plate and the granular medium. This completes the first iteration.

Then, the computation proceeds to the second iteration at the time instant τ_{s+1}, setting $j = 2$ and repeating the previous two phases, and so on. In essence, at each step of the iteration at the (fixed) time instant τ_{s+1} we evaluate the responses of the rigid layers at the boundary of the plate (during the first phase of the iteration), and then compute the response of the granular medium for $\tau \in [\tau_s, \tau_{s+1}]$ assuming that the rigid layers at the plate are acting as moving boundaries (at the second phase of the iteration). Ultimately, this iterative scheme generates a *nonlinear map* relating the j-th iterates of the interaction forces applied to the rigid layers on the plate to the corresponding $(j + 1)$ th iterates, or, in symbolic form, $\left[\boldsymbol{N}_{s+1}^{(j)}, \boldsymbol{f}_{s+1}^{(j)}\right] \to \left[\boldsymbol{N}_{s+1}^{(j+1)}, \boldsymbol{f}_{s+1}^{(j+1)}\right]$ at the current time step τ_{s+1}. With increasing iterations, the interaction forces are expected to converge, as discussed in "Appendix 1". Supposing that convergence is achieved at the J-th iteration, we denote the converged interaction force vectors at the time instant τ_{s+1} as, $\left(\boldsymbol{N}_{s+1}^C, \boldsymbol{f}_{s+1}^C\right) \equiv \left(\boldsymbol{N}_{s+1}^{(J)}, \boldsymbol{f}_{s+1}^{(J)}\right)$. Once the interaction forces applied to the plate have converged, the plate and granular medium responses at the current time step τ_{s+1} will have converged as well, and the computation proceeds to the next time step τ_{s+2}, where the outlined iteration scheme is re-initiated. This is repeated until the entire time interval T of the simulation is exhausted and completes the computational algorithm according to the flow chart of Fig. 13.

Central to the numerical convergence of the computational algorithm is the stability of the global map $\left[\boldsymbol{N}_{s+1}^{(j)}, \boldsymbol{f}_{s+1}^{(j)}\right] \to \left[\boldsymbol{N}_{s+1}^{(j+1)}, \boldsymbol{f}_{s+1}^{(j+1)}\right]$ generated by the iterations. This issue is discussed in detail in "Appendix 1", so here we provide a synopsis of a set of theoretically predicted conditions to ensure convergence. To start with, to ensure the convergence of the β-Newmark method, the time step increment $\Delta\tau$ should be sufficiently small so that variations of the interaction forces at a contact point has negligible effects on the responses at the other contact points at the current time instant τ_{s+1}. It follows that, since the interaction forces at a contact point of the plate have a local effect, the next iteration of the interaction forces at that contact point should also be determined solely by the local response at the contact point. Accordingly, the global map $\left[\boldsymbol{N}_{s+1}^{(j)}, \boldsymbol{f}_{s+1}^{(j)}\right] \to \left[\boldsymbol{N}_{s+1}^{(j+1)}, \boldsymbol{f}_{s+1}^{(j+1)}\right]$ can be decomposed into individual 2D local maps $\left(N_{k,s+1}^{(j)}, f_{k,s+1}^{(j)}\right) \to \left(N_{k,s+1}^{(j+1)}, f_{k,s+1}^{(j+1)}\right)$ at each contact point (say k) at the current time step. Clearly, *the global map is stable if all 2D local maps are stable* (i.e., for every contact point k on the plate). Following the analysis in "Appendix 1", the 2D local map is stable if the moduli of both of its linearized eigenvalues are smaller than unity. Moreover, as an approximation we can use the converged data of the previous time step to judge whether the iteration is stable or not at the current time step. Therefore, the conditions for convergence of the local map can be formulated as follows,

$$\left|\lambda_{k1,s+1}\right| = \frac{1}{2}E^*\sqrt{R^*}\Delta\tau^2\boldsymbol{T}_{k,n}\left(\boldsymbol{M} + \frac{1}{4}\boldsymbol{K}\Delta\tau^2\right)^{-1} \boldsymbol{T}_{k,n}^T\left(u_{k,p,n,s}^C - u_{k,b,n,s}^C\right)_+^{1/2} < 1 \tag{13a}$$

$$|\lambda_{k2,s+1}| = \frac{1}{2}\mu k_s \left| N_{k,s}^C \right| \Delta\tau \boldsymbol{T}_{k,t} \left(\boldsymbol{M} + \frac{1}{4}\boldsymbol{K}\Delta\tau^2 \right)^{-1} \boldsymbol{T}_{k,t}^T \cosh\left[k_s \left(v_{k,p,t,s}^C - v_{k,b,t,s}^C \right) \right]^{-2} < 1 \tag{13b}$$

where $\lambda_{k1,s+1}$ and $\lambda_{k2,s+1}$ are the linearized eigenvalues of the local map $\left(N_{k,s+1}^{(j)}, f_{k,s+1}^{(j)}\right) \rightarrow \left(N_{k,s+1}^{(j+1)}, f_{k,s+1}^{(j+1)}\right)$ and the k-th contact point and time instant τ_{s+1}. Clearly, for convergence of the algorithm the conditions (13a, b) should apply at every contact point and at every time step τ_{s+1}. In (13a, b) superscript C denotes the converged value at the previous time instant τ_s, $\Delta\tau$ the time step, $\left(u_{k,p,n,s}^C - u_{k,b,n,s}^C\right)$ and $\left(v_{k,p,t,s}^C - v_{k,b,t,s}^C\right)$ the relative normal displacement and tangential velocity, respectively, between the plate and the contacting granule at the $k-th$ contact point, and $\boldsymbol{T}_{k,n}$, $\boldsymbol{T}_{k,t}$ are sparse vectors whose only non-zero terms, equaling unity, are located at the normal and tangential driving DOFs at the $k-th$ contact point, respectively. Lastly, from the previous notation, $N_{k,s}^C$ denotes the converged normal force applied at the $k-th$ contact point (node) on the plate at the time instant τ_s. Note that the convergence criteria (13a, b) are formulated in terms of the response at all contact points k on the rigid layers of the plate. The criteria (13a, b) can be conveniently checked at each iteration and time step *in tandem* with the main computation of the interaction forces and responses.

Based on the conditions (13a, b) the critical value for the time step $\Delta\tau$ for convergence of the computation can be estimated at each time instant. Note that as the friction coefficient tends to infinity, $k_s \rightarrow +\infty$, and $v_{k,p,t,s}^C - v_{k,b,t,s}^C \rightarrow 0$, the critical time step tends to zero, $\Delta\tau \rightarrow 0$. Therefore, *the Coulomb friction model (obtained in the limit of the current Coulomb-tanh friction model as $k_s \rightarrow +\infty$) leads to divergence of the computational algorithm*. This was confirmed by direct numerical simulations. Following this reasoning, in the following applications of the computational algorithm we select k_s such that $k_s v_{ch} \gg 1$, where v_{ch} is a characteristic velocity of the acoustics. As discussed in [55] a sufficiently large value of k_s yields results close to the Coulomb friction model; however, if k_s becomes exceedingly large, in practice it is more difficult for the iteration algorithm to converge. Similarly, the iteration algorithm has convergence problems for any discontinuous friction model. On the contrary, based on (13a, b) the numerical algorithm can easier converge for larger local mesh sizes of the plate close to the contact points, and/or smaller interaction forces applied to the plate. Hence, parameters such as, the time step $\Delta\tau$, the friction parameter k_s, and the local mesh size may be regarded as important control parameters affecting the convergence of the algorithm. In a physical context, the convergence relations (13b) indicates that the critical value of the time step may occur when the relative tangential velocity at the interface is close to zero, where the friction force is highly sensitive to the local relative velocity.

4 Application to specific a granular-solid interface

We now demonstrate the efficacy of the computational algorithm and, in the process, test the validity of the previous theoretical convergence analysis. To this end, we consider the 2D granular-solid interface of Fig. 4, composed of a thin plate and an ordered granular medium with fourteen hexagonally placed granules, of which the five right boundary granules are in contact with the edge of the plate. The top and bottom edges of both the granular medium and the plate are assumed to be clamped (fixed), and the right edge of the plate traction-free. The middle region of the left edge of the plate is in contact with the granular medium, while the remaining region of the left edge of the plate is clamped as well. Uniform impulse excitations are applied to the left granules of the granular medium at $\tau = 0$, and the state of the system at $\tau = 0-$ is zero; this amounts to imposing uniform initial velocities equaling v_0 to the five left granules of the medium at $\tau = 0+$.

Following [49], the friction and damping coefficients of the granular medium are selected as $\mu = 0.099$—cf. relation (5), and $\alpha_n = 6.313 \times 10^{-3}$—cf. relation (3), respectively. Unless otherwise noted, the intensity of the uniformly applied impulse is selected so that $v_0 = 0.5$ m/s. This level of impulse intensity ensures that the elastic strains and stresses, and contact forces in the granule-to-granule and granule-to-plate interactions are within the elastic limit of the material and fulfill the requirements of DE modeling of the granular medium [6]. Given that the rigid layers on the plate in contact to the granular medium should be much smaller than the (common) radius of the granules, R, their lengths are selected as $R/10$, a value which is comparable to the maximum expected contact diameter at the interface (cf.

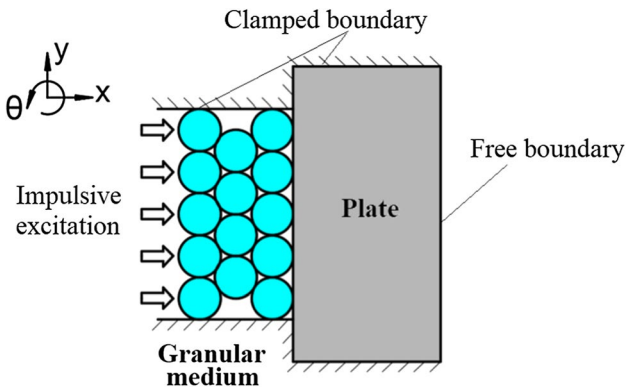

Fig. 4 The granular-solid interface considered in the application

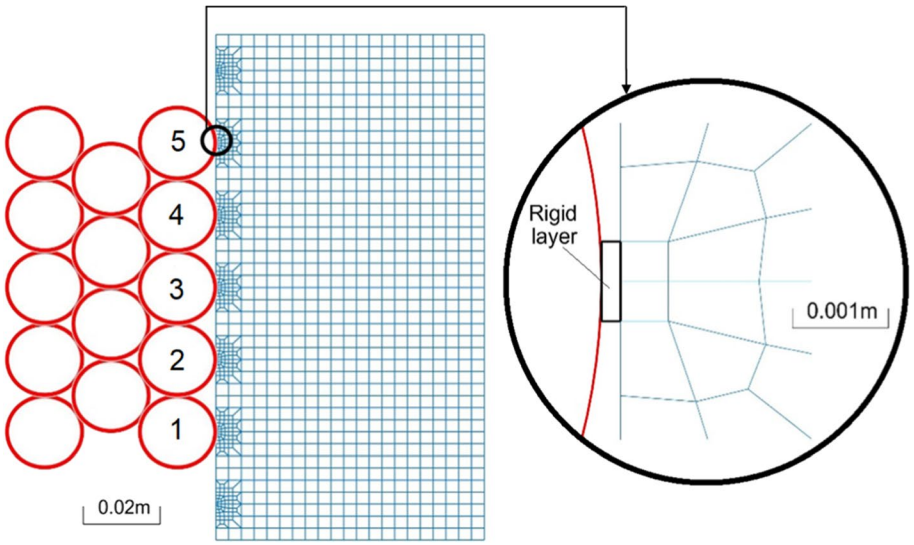

Fig. 5 Variable FE mesh topology for the thin plate—the detail shows the local topology of the mesh close to each contact point

Table 1 System parameters of the granular-solid interface (cf. Fig. 4)

Elastic modulus	Poisson's ratio	Granule radius	Plate thickness	Plate lateral dimensions	Material density
200 GPa	0.3	0.01 m	0.005 m	0.07 m×0.14 m	7850 N/m^3

Fig. 5). In addition, considering $v_{ch} = v_0$ as the characteristic velocity of the acoustics and imposing the convergence requirement $k_s v_0 \gg 1$, we select the Coulomb-tanh friction model parameter as $k_s = 100$ s/m. We note that the same numerical value for this parameter was used also in [55], with the results obtained by the Coulomb-tanh model being close to those obtained by the Coulomb model. Finally, for simplicity we designate the boundary granules in contact with the edge of the plate as "granules 1–5" (cf. Fig. 5). Lastly, both the granular medium and the elastic plate are made of steel, and their geometrical and material parameters are listed in Table 1.

The FE mesh for the thin plate is depicted in Fig. 5. To ensure accuracy and convergence of the computational algorithm, we considered a variable-size FE mesh, with smaller finite elements being placed in the neighborhoods of the five contact points. At each contact point, the two smallest plate finite elements are the ones attached to the rigid layer; these have dimensions $\left(5 \times 10^{-4}\right) \times \left(5 \times 10^{-4}\right)$ m^2, whereas the rigid layer has negligible thickness and length 1×10^{-3} m (cf. detail in Fig. 5). Taking into account that the speed of sound in the steel plate is nearly 5700 m/s, in the initial simulation we consider the constant time step, $\Delta\tau = 2 \times 10^{-8}$ s, to best capture the nonlinear stress wave transmission across the granule-plate interface. The total simulation time is set to $T = 0.2$ ms. A preliminary estimation indicates that for the expected range of relative normal displacements and tangential velocities at the granular-solid interface, the first convergence condition (13a) is always satisfied; *therefore it is the second convergence criterion* (13b) *that solely determines the convergence of the algorithm.*

Before we test the efficacy of the computational algorithm, we introduce an additional energy-based convergence measure that, apart from the benefit of being physics-based, it provides a direct measure of the accuracy and consistency of the numerical results at each time step. To this end, at each time instant of the computation we compute the total instantaneous energy of the granular-solid interface by adding, (i) the total instantaneous energy (potential and kinetic) of the granular medium—cf. relations (7a, b), (ii) the total instantaneous energy of the plate—cf. relations (12a, b), (iii) the cumulative energy dissipated by structural (viscous) damping in the granules up to that time instant—cf. relation (8b), and (iv) the cumulative frictional energy dissipated due to relative rotations at granule-to-granule and granule-to-plate interfaces up to that time instant—cf. relation (8a). Note that we have neglected any dissipative effects in the steel plate, as its structural damping is very low (compared to the granular medium), and since we are only interested in the early-time propagation of the stress wave front where the effects of dissipation in the plate are expected to be minimal due to the relatively fast wave speed in that medium. To ensure accuracy and convergence of the computation, *at each time instant the previous summation of energies should be equal to the total input energy induced by the impulsive excitation*. This type of convergence criterion based on energy preservation will prove to be highly efficacious for the following highly nonlinear and discontinuous acoustics of the granular-solid interface.

The results of the simulation are depicted in Fig. 6. In Fig. 6a we show the instantaneous energies of the granular medium and the plate, as well as the total instantaneous

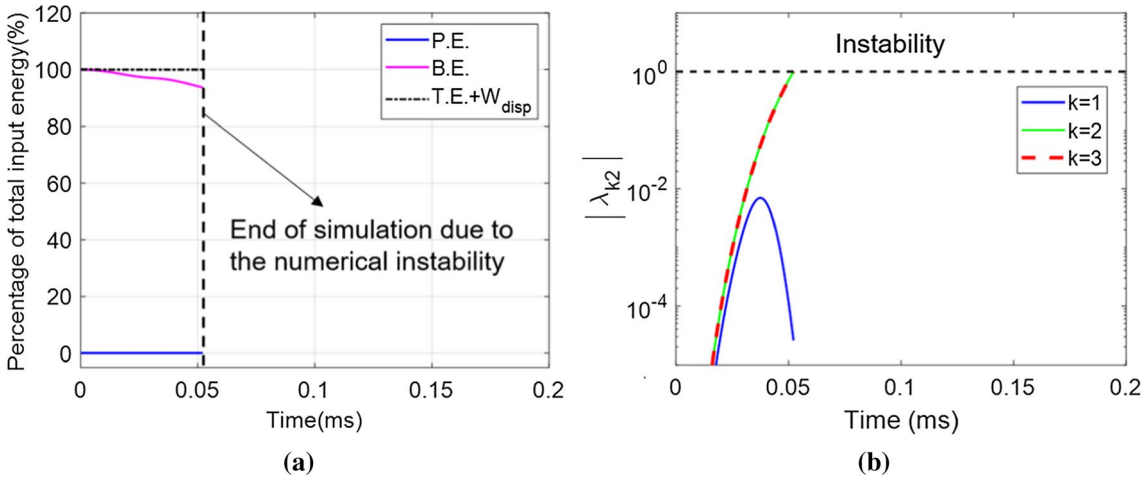

Fig. 6 Initial simulation with fixed time step $\Delta\tau = 2 \times 10^{-8}$ s: **a** Instantaneous energies of the granular medium (purple curve) and plate (blue curve), respectively, and total instantaneous energy (black line) that includes dissipative effects; **b** eigenvalue moduli $|\lambda_{k2}|, k = 1, 2, 3$ computed from relation (13b)

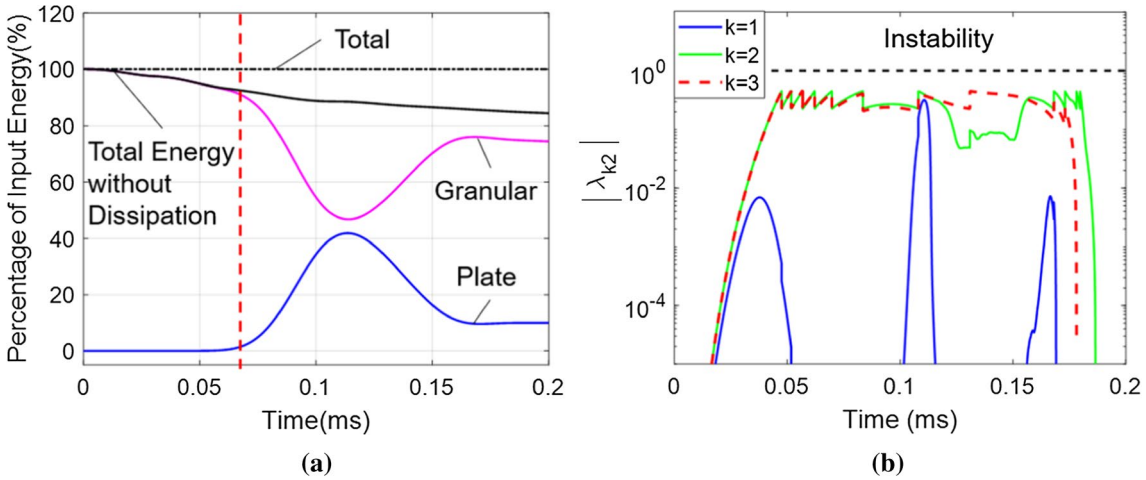

Fig. 7 Simulation with self-adaptive time step, $v_0 = 0.5$ m/s: **a** Instantaneous energies of the granular medium (purple curve) and plate (blue curve), respectively, and total instantaneous energy (black line) that includes dissipative effects; **b** eigenvalue moduli $|\lambda_{2k}|, k = 1, 2, 3$ from (13b); dashed line indicates the arrival of the primary stress wave front at the granular-plate interface

energy of the entire interface, which, since it includes the dissipated energy, is preserved at each instant of time. Note that the simulation ends at ~ 0.055 ms since at then the algorithm cannot converge and yields numerical instability. Yet, the total energy preservation convergence criterion holds before the simulation stops, verifying the accuracy of the simulation before the onset of numerical instability. The validity of the convergence condition (13b) is shown in Fig. 6b, which depicts the moduli of the three eigenvalues $\lambda_{k2}, k = 1, 2, 3$, at the corresponding contact points (due to the symmetry of the interface and the uniform load distribution we only need to consider three of the five contact points). We deduce that, as predicted in the previous Section, at the time instant when the modulus of at least one of the eigenvalues (13a, b) exceeds unity, the iteration scheme ceases to converge. This result validates the theoretical stability analysis and highlights its predictive capacity. Furthermore, it proves that even very small, but fixed, time steps may introduce numerical instability.

To eliminate the numerical instability, we change to a self-adaptive (variable) time step while still keeping the maximum time step to 2×10^{-8} s. To this end, at each time instant of the computation the *critical* time step increment $\Delta\tau_{cr}$ is calculated based on the convergence condition (13b), and the *actual* time step is chosen to be smaller than the critical one, $\Delta\tau < \Delta\tau_{cr}$; according to the previous convergence

analysis this should ensure the convergence of the interaction force vector at the given time instant. Since the critical time step varies with time, the actual time step will be self-adaptive. The computational results with self-adaptive time step are depicted in Fig. 7. Note that total energy remains constant at each time instant, verifying the accuracy and robustness of the numerical computation. Moreover, the results depicted in Fig. 7b confirm that the computational algorithm converges at all time steps, given that the moduli of the eigenvalues λ_{2k} at all contact points remain smaller than unity.

From Fig. 7a we note that there occur intense energy exchanges between the granular medium and the plate, starting at $\tau \sim 0.7$ ms when the early-time stress wave front propagating through the granular medium reaches the boundary with the plate. Following this, the total energy in the plate reaches its maximum at $\tau \sim 0.12$ ms, while at $\tau \sim 0.17$ ms the energy exchange stops as all five boundary granules (1–5) lose contact with the plate boundary. At the time of loss of contact the residual energy that is localized in the plate is small, namely, only about 10% of the total impulsive energy; the energy of the plate remains at this constant low level until the boundary granules (or a subset of them) regain contact with the plate, at which time the energy exchanges between the granular medium and the plate resume. This, however, occurs at a much later time instant, not shown in Fig. 7. Finally, we note that the frictional and structural damping effects in the granular medium dissipate a moderate portion of the input energy, which steadily increases with time.

To gain further insight into the nonlinear acoustics of the wave transmission through the granular-solid interface, in Fig. 8 we depict successive early-time snapshots of the spatial distributions of the total instantaneous energy densities of the granular medium and the plate. A normalization is introduced so that the initial energy densities of the left granules (the ones directly excited by the applied impulsive loads) are equal to unity:

$$\hat{w} = \frac{w}{w_0} = w \cdot \left[\frac{(1/2)m_b v_0^2}{V_b}\right]^{-1} = w \cdot \left[(1/2)\rho_b v_0^2\right]^{-1} \tag{14}$$

In (14) $\hat{w}$ and w denote normalized and unnormalized energy density, respectively, V_b and m_b the volume and mass

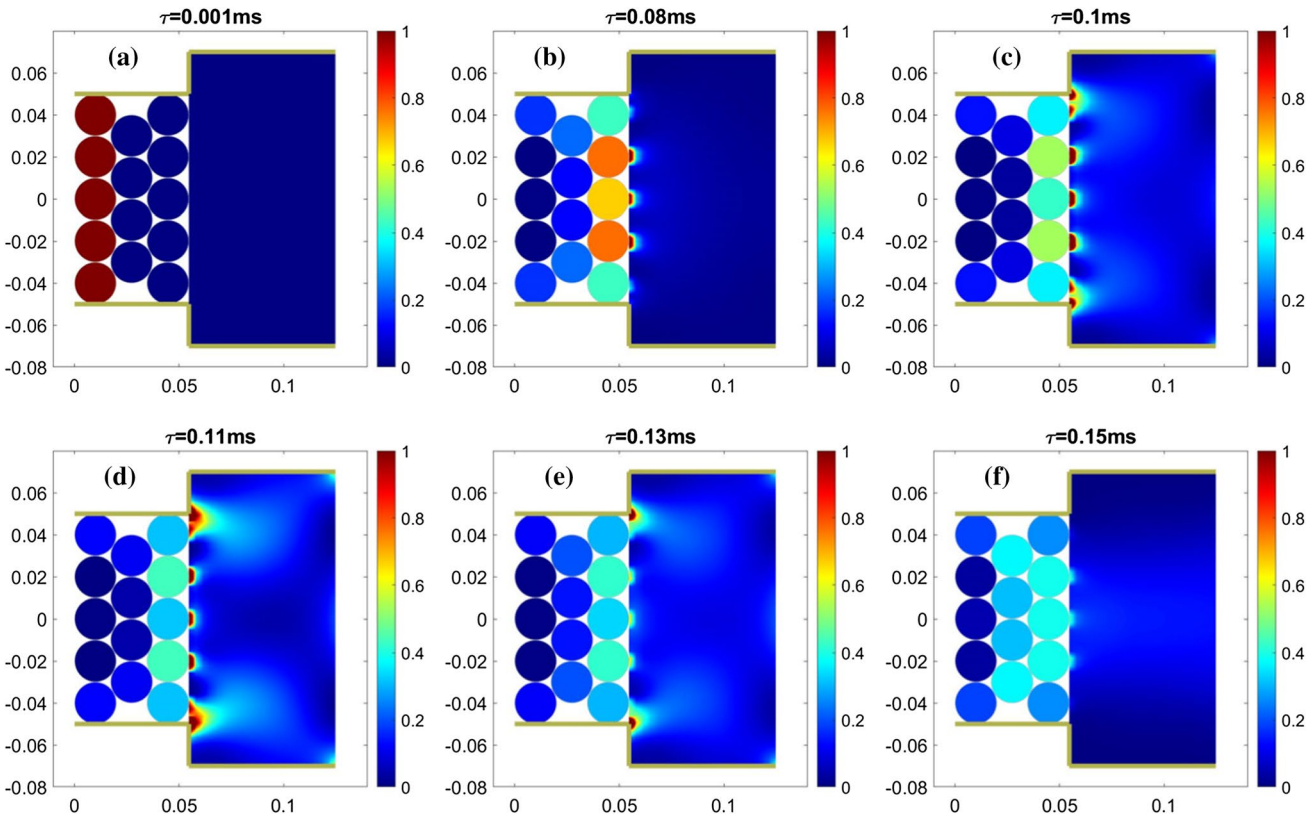

Fig. 8 Snapshots of normalized energy density $\hat{w}$ of the granular-solid interface for $v_0 = 0.5$ m/s: **a** $\tau = 0.001$ ms, **b** $\tau = 0.08$ ms; **c** $\tau = 0.10$ ms, **d** $\tau = 0.11$ ms, **e** $\tau = 0.13$ ms, and **f** $\tau = 0.15$ ms; note that at the later-tame snapshots (**d**–**f**) secondary wave reflections have already occurred from the boundaries of the plate

of each granule, respectively, and v_0 the initial velocity of the five left granules at $\tau = 0+$. For the granular medium, the energy density of each granule is computed as $w_b = E_{bi}/V_b$, where E_{bi} denotes the total instantaneous energy of the i-th granule—cf. relation (7a). For the plate, the energy density is defined as $w_p = \left[E_e/\left(A_e t\right)\right]$, where E^e denotes the total instantaneous energy of a specific finite element—cf. relation (12a), A_e the area the finite element, and t the thickness of the plate.

A first observation is that, since the boundary conditions at the left boundary of the plate are not continuous, intense stress concentration occurs at the points of discontinuity where the energy density attains relatively large values. Primary wave transmission from the granular medium to the plate is depicted only in the early-time snapshots, namely Fig. 8a–c, that is, before the primary wave front has undergone secondary reflections from the plate boundaries. Examining in more detail the transmitted wave front, we note that most of the energy transmitted from the granular medium to the plate occurs through the three middle contacting granules 2–4. This is especially evident when one considers the snapshot of Fig. 8b corresponding to $\tau = 0.08$ ms, where intense "focusing" of the shock energy in granules 2 and 4—and to a lesser extent in granule 3—is deduced. The capacity of the granular medium for nonlinear focusing (or defocusing) of propagating waves (and energy), is one of the most interesting aspects of its acoustic and can be beneficial in its application as passive shock mitigator.

Another interesting aspect of the nonlinear acoustics in the granular-solid interface is deduced when we consider the partition of the instantaneous energy of its two constituent parts in terms of kinetic and potential energy. In Fig. 9a, b we depict the normalized instantaneous kinetic, potential and total energies in the granular medium and the plate, respectively. It is interesting to note that the 2D granular medium acts nearly as a "global (nonlinear) oscillator", given the coherent exchange between its kinetic and potential energies in a single cycle during the simulation period $0 < \tau < 0.2$ ms. No such exchange is realized in the (linear) plate, where its energy is mainly potential, with a small residual kinetic energy component (cf. Fig. 9b). The "global oscillator" behavior is even more evident in Fig. 9c where the entire granular-solid interface is considered; hence, it appears that the granular medium introduces a remarkable coherence in the entire early-time acoustics of the interface. *The striking behavior of the granular medium as a coherent global nonlinear oscillator might explain its capacity to confine (localize) and locally dissipate a major portion of the induced impulsive energy, while "releasing" only a small portion of it to the plate, mainly in the form of potential energy*. Previous studies (e.g., [62, 63]) have demonstrated both theoretically and experimentally the capacity of nonlinear oscillators for energy localization and motion confinement.

The previous findings are corroborated by the energy plots of Fig. 7a, where the maximum percentage of the applied shock energy transmitted to the plate is nearly 41%, with a moderate part of shock energy being dissipated by frictional and structural damping in the granular medium, and a larger part being confined (localized) in the granular medium itself. Moreover, as time progresses and the secondary reflected wave from the right boundary of the plate reaches the boundary with the granular medium, a large portion of the shock energy backscatters from the plate to the granular medium, so by the time of loss of contact of the boundary granules (at $\tau \sim 0.17$ ms—not shown in Fig. 8), as low as $\sim 10\%$ of the input shock energy remains in the plate;

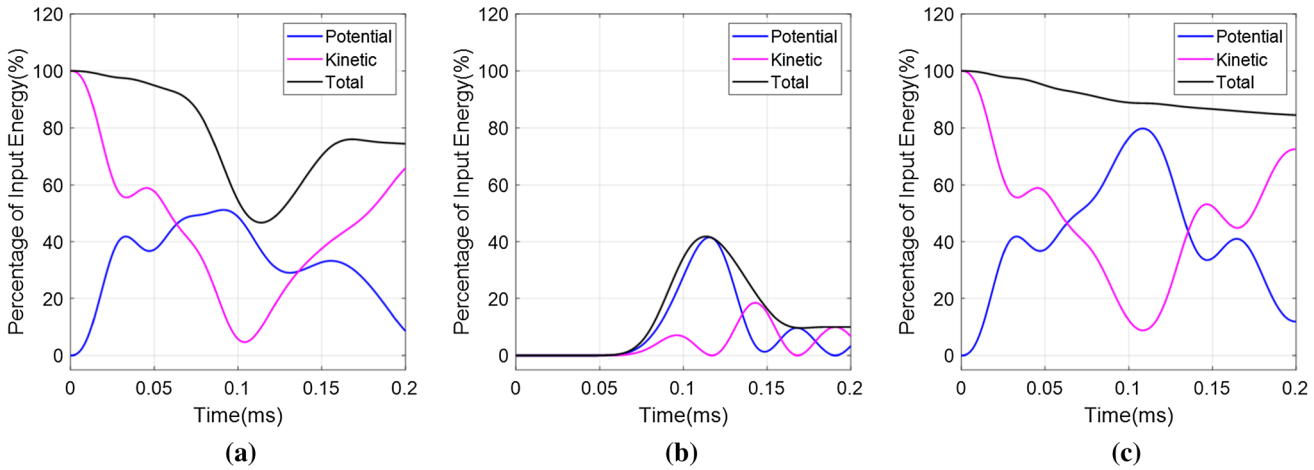

Fig. 9 Instantaneous energy partition in the granular-solid interface in terms of kinetic and potential energies in the **a** 2D granular medium, **b** plate, and **c** entire granular-solid interface, for $v_0 = 0.5$ m/s

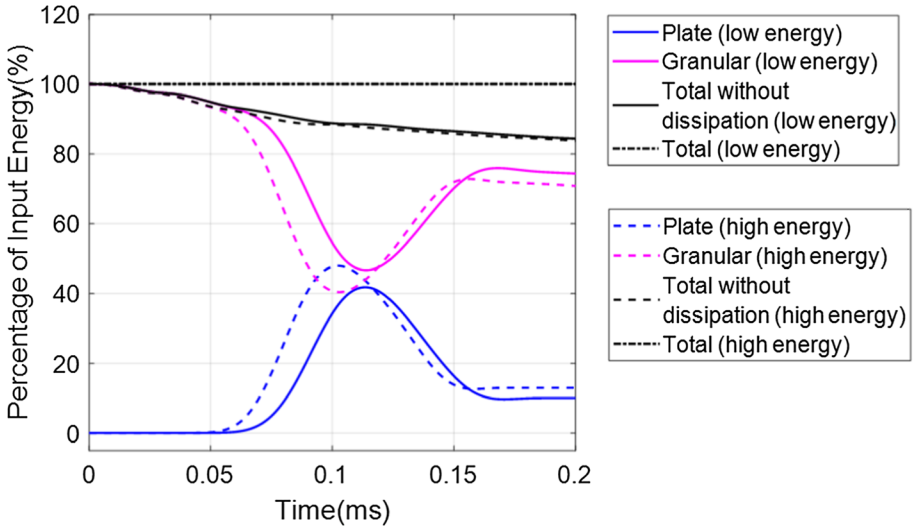

Fig. 10 Instantaneous energies of the granular medium and the plate, and total instantaneous energy with/without dissipative effects, for $v_0 = 0.5$ m/s (low energy) and $v_0 = 1.0$ m/s (high energy); note the dependence of the acoustical response on the intensity of the applied shock

of course this energy confinement is not permanent, since at a later time the boundary granules regain contact.

These acoustical phenomena originate from the strongly nonlinear and highly discontinuous nature of the granule-to-granule and granule-to-plate interactions, and as shown below, greatly enhance the shock mitigation capacity of the granular-solid interface. What is even more noteworthy is that *the nonlinear acoustics of the interface is self-adaptive to (or tunable with) the applied shock excitation*; that is, the wave transmission and scattering in the granular-plate interface is dependent on the intensity level of the applied shock excitation, and on its frequency and wavenumber content. This is an additional interesting feature of the nonlinear acoustics, which, however, is typical of the highly nonlinear granular medium studied herein, e.g., cf. [6]. Since in the considered the applied shock is uniform in space and idealized in time (as it is generalized a delta-function), in what follows we will highlight only the dependence of the nonlinear acoustics on energy, that is, by varying the intensity of the applied shock excitation.

To this end, we reconsider the granular-solid interface of Fig. 4, but now consider a higher-intensity load of uniform impulses corresponding initial velocity $v_0 = 1.0$ m/s for the left boundary granules; this will be referred to as the "high energy case" in Fig. 10. For comparison, in the same plot we reproduce the energy plots of Fig. 7a for $v_0 = 0.5$ m/s, which we will designated as the "low energy case". We note that in the higher energy case the wave transmission in the granular medium is faster, so that energy exchange with the plate starts occurring earlier; this clearly highlights the energy dependence of the speed of the propagating stress wave in the 2D hexagonally ordered granular medium, which results due to the nonlinear constitutive relation and the discontinuous topology of the medium itself. In the high energy case, the energy transmitted in the plate reaches its maximum at $\tau \approx 0.1$ ms (earlier than the lower energy case), while a larger proportion of the initial impulsive energy is now transmitted to the plate at that time instant. Moreover, at the high energy case, a slightly higher portion of the impulsive energy gets "trapped" in the plate after the right boundary granules of the medium loose contact at $\tau \approx 0.15$ ms.

In the next numerical simulations, we highlight the capacity of the granular medium to drastically "delay" the early-time transmitted wave through the interface, and strongly disperse it, thus greatly attenuating the intensity of the wave that is eventually transmitted to the plate. These additional nonlinear features of the granular medium demonstrate its efficacy as effective shock mitigator. To this end, we consider a "monolithic" plate system, composed of the plate of the system of Fig. 4 (labelled the "right" plate), but with the granular medium replaced by a "left plate" of lateral dimensions analogous to the 2D granular medium, and material-thickness properties identical to the right plate (cf. Fig. 11a). Furthermore, the boundary conditions of the monolithic system are analogous to the granular-solid interface (cf. Fig. 11a, c). The resulting system is linear and homogeneous, and, under identical shock excitation can be used to compare the wave transmission to the granular-solid interface. Given that the response of the monolithic system is computed by FE discretization, it is not possible to apply a uniformly distributed impulse load as in the granular medium of Fig. 4. To this end, a uniformly distributed impulse is applied at the left boundary of the left plate in the form of a half-sine force in time. The duration of the impulse is 1 μs and its intensity, 20000 N/m. Since the duration of the applied force is much smaller than the anticipated time scale of the wave propagation, we may consider this loading condition as a good approximation of an idealized impulse (that is instantaneously applied). This corresponds to input energy by the shock equal to 0.0096 J. For a fair comparison,

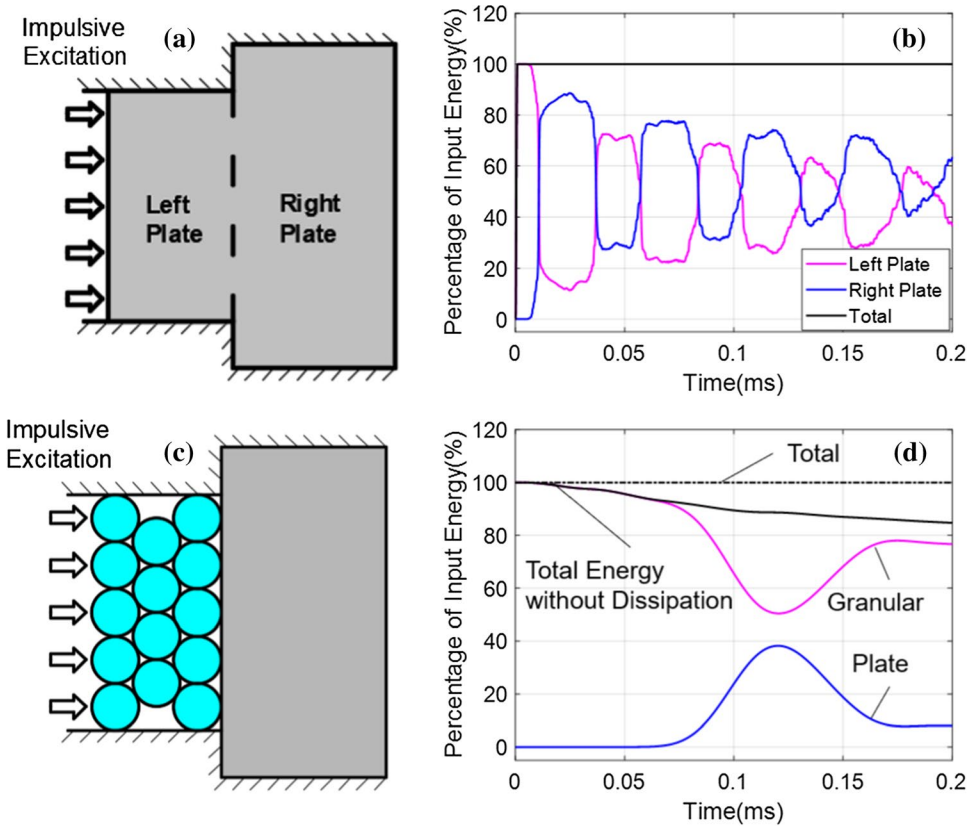

Fig. 11 Comparison of the responses of the "monolithic" plate system and the granular interface subject to same energy impulsive loads: Configuration and energy transmission measures of (**a**, **b**) the monolithic plate system, and (**c**, **d**) the granular-solid interface

the exact same amount of input energy is considered for the impulsive loading at the granular-solid interface (cf. Fig. 4) corresponding to an initial velocity of $v_0 = 0.3414$ m/s for its five left granules. Under such "equal forcing" conditions, we wish to compare the transmitted energy in the monolithic system to the corresponding energy in the granular-solid interface.

In Fig. 11b we depict the instantaneous total energies in the left and right plates of the monolithic system and compare them to the corresponding energy measures for the granular-plate interface depicted in Fig. 11d the for the same time window. Note that since we neglect dissipative effects in the monolithic plate system, its total instantaneous energy is conserved. The comparison of these results shows that *the 2D granular medium inflicts a drastic delay in the primary propagating front*; indeed, whereas in the monolithic system the primary stress wave reaches the left boundary of the right plate in less than 0.01 ms, in the granular-plate interface the time of arrival of the wave front at the plate boundary increases to ~ 0.07 ms. Clearly, this significant time delay is caused by the highly discontinuous and nonlinear stress wave transmission through the hexagonal 2D granular medium, and also by its capacity to redirect a portion of the shock energy in a direction normal to the main (axial) direction of wave propagation (cf. Fig. 9). The resulting intense nonlinear wave dispersion in the granular medium is reflected by the highly diminished transmitted energy in the right plate of the granular-plate interface, with the maximum energy transfer reaching $\sim 39\%$ of the initial impulsive energy, compared to $\sim 88\%$ for the monolithic plate system. A last comment regards the time scales governing the acoustics of the systems considered. Comparing the energy transmission plots of Fig. 11b, d we deduce that the linear acoustics of the monolithic plate system is governed by faster time scales (or higher frequencies) compared to the strongly nonlinear (and energy-tunable) acoustics of the granular-solid interface. In fact, the 2D granular medium appears to greatly "soften" the acoustics, compared to the much "stiffer" acoustics of the monolithic plate system.

Lastly, in Fig. 12 we demonstrate more clearly the time delay and strong dispersion in the acoustics caused by the 2D granular interface, by comparing certain snapshots of the normalized energy density $\hat{w}$ of the previously discussed granular-solid interface and the monolithic plate system. The snapshots of Fig. 12a, c depict the arrival of the primary stress wave front at the granular-plate interface, and the boundary between the left and right plates of the monolithic system, respectively. We note that, whereas in the granular-solid interface most of the energy of the early-time wave front gets strongly dispersed in the granular medium before it reaches the interface with the plate, in the case of the monolithic system most of the impulsive energy remains

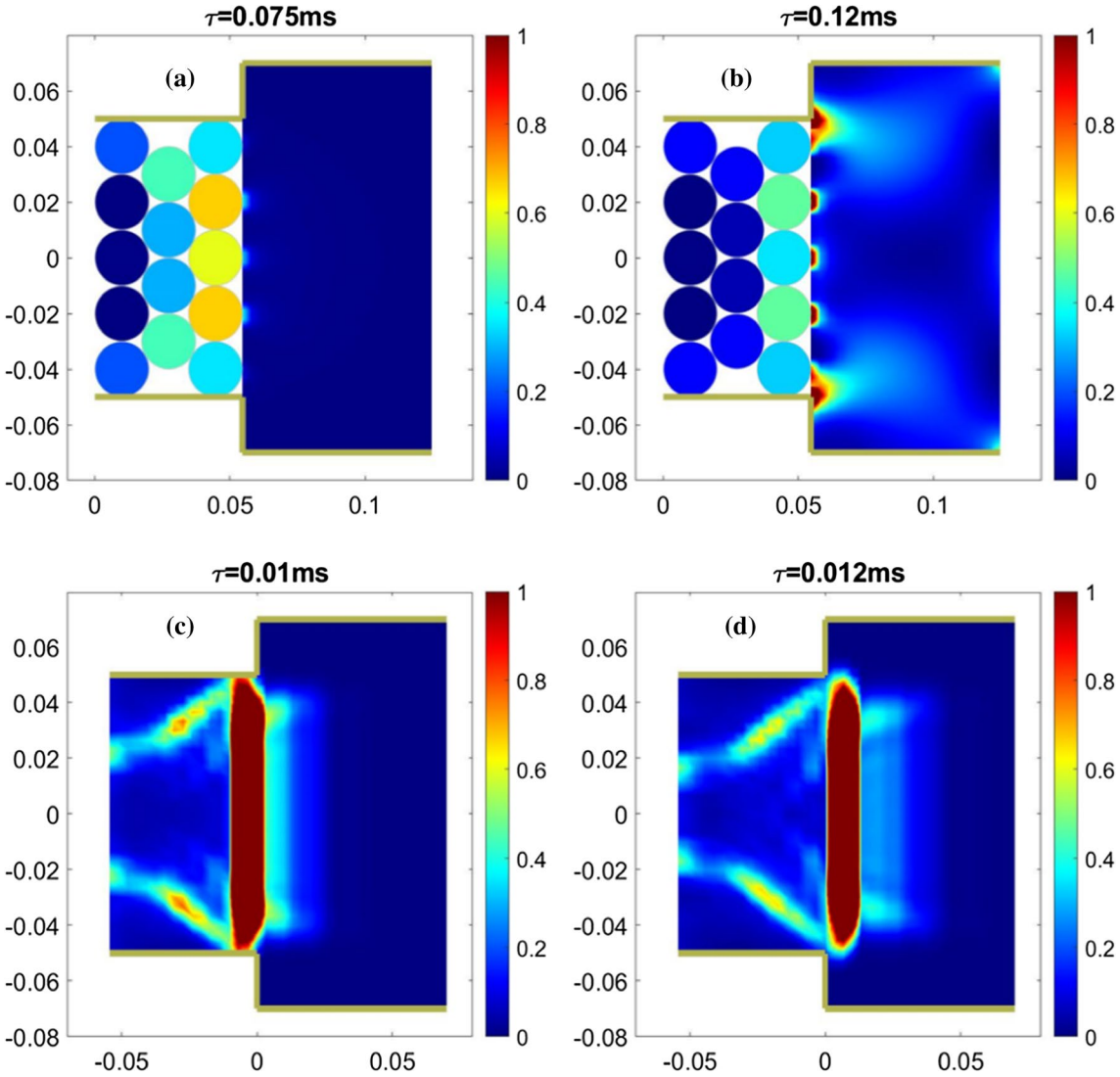

Fig. 12 Snapshots of normalized energy density $\hat{w}$ of the (**a**, **b**) granular-solid interface for $v_0 = 0.341$ m/s at $\tau = 0.075$ ms and $\tau = 0.12$ ms, respectively, and (**c**, **d**) monolithic plate system subject to same-energy impulsive loads at $\tau = 0.01$ ms and $\tau = 0.012$ ms, respectively; the results show the time delay and strong dispersion in the acoustics due to the 2D granular medium

localized in the primary wave front throughout the early-time wave transmission. Therefore, contrary to the monolithic plate system where most of the impulsive energy gets transmitted from the left plate to the right in a high-intensity primary wave front (indicated by the high-intensity localized energy areas in Fig. 12c, d), in the granular-plate interface only a small portion of the impulsive energy gets eventually transmitted to the plate—cf. snapshots of Fig. 12b, d. In the latter case, the intensities of the disjoint wave fronts that eventually reach the plate are small, due to the strong nonlinear wave dispersion in the granular medium.

In "Appendix 2" we provide links for animations of the acoustics described in Figs. 11 and 12. Specifically, we provide an animation for the linear acoustics of the monolithic plate of Fig. 11a subject to a uniform impulse of 1 μs and 20000 N/m intensity; this is compared to an animation of the nonlinear acoustics of the granular-solid interface of Fig. 11c with uniform impulsive loading corresponding to uniform initial velocities $v_0 = 0.3414$ m/s of its five left granules. As mentioned previously, in both systems the input impulsive energy equals 0.0096 J. To highlight the tunability of the nonlinear acoustics to the intensity of the impulse, in "Appendix 2" we include two additional animations of the granular-solid interface of Fig. 11c with uniform initial velocities $v_0 = 0.5$ m/s and $v_0 = 1.0$ m/s of its five left granules.

These results conclude the application of the computational code. Summarizing, we proved the validity of the theoretical convergence measures of Sect. 3 and showed that the computational algorithm can be applied to accurately

and robustly solve highly complicated acoustical problems involving the interactions of 2D granular media and their flexible boundaries. Moreover, the numerical analysis carried out for this application shed valuable physical insight into the highly nonlinear and discontinuous acoustics of 2D ordered granular media and underscored the efficacy of utilizing such media as effective passive shock mitigators.

5 Concluding remarks

We studied the strongly nonlinear wave transmission in 2D granular-plate interfaces subject to shock excitations, taking into account not only the highly discontinuous Hertzian granule-to-granule and granule-to-plate interactions, but also the frictional effects due to relative granular and granular-plate rotations. Friction effects are especially challenging to model, given that they can give rise to numerical instabilities; yet there is the need to take them into full consideration to ensure the accuracy of the computational results. To the authors' best knowledge, the present is the first study in the literature that addresses granular-elastic solid interfaces in two dimensions taking into account the combined frictional and Herzian effects.

To study this challenging problem, we formulated a computational algorithm based on interrelated iterative and interpolative schemes, in conjunction with a set of predictive convergence criteria that informed the appropriate parameter selection that ensured robustness and stability of the computation. These convergence criteria were theoretically derived by studying the linearized eigenvalues of local nonlinear maps governing the interaction forces that coupled the granular medium and the plate at successive time steps. The validity of the resulting self-adaptive algorithm was tested with a specific granular-plate interface. The application demonstrated the efficacy of the computational approach to accurately and robustly predict the highly complex patterns of transmitted and reflected stress waves at the discrete-continuum interface. Moreover, the developed computational algorithm could serve not only as useful and predictive tool for engineering complex granular-solid interfaces, but also can be extended to a broader class of problems in engineering and physics involving discrete-continuum interfaces (e.g., granular flows in containers with flexible walls, shock/blast protection systems, etc.).

The application of the self-adaptive computational algorithm reported herein already provided interesting findings on the nonlinear acoustics of granular-plate interfaces, but at the same time posed some important open questions that dictate further investigations. A first finding was that the 2D hexagonal granular medium inflicts drastic time delay to the wave transmitted to the plate due to significant "softening" of the acoustics compared to the "monolithic" plate system. This is accompanied by shock energy localization, nonlinear dispersion and effective dissipation in the granular medium itself, with only a relatively small portion of the shock energy being eventually "released" to the plate at a relatively slow time scale. The causes for this significant nonlinear dispersion in the granular medium can be only surmised at this point; e.g., the nonlinear motion confinement in the granular medium might be caused by the entire granular-medium interface acting coherently as a "global nonlinear oscillator"; in addition, there is possible directed energy transfer within the granular medium in directions orthogonal to the axial direction of main energy propagation; or there is the possibility that the highly discontinuous and nonlinear granule-to-granule and granule-to-plate Hertzian and frictional interactions drastically delay the wave transmission, enhance nonlinear wave dispersion and reduce the energy transmission to the plate. Clearly, more research is required to answer interesting questions like these.

An additional promising prospect is to consider granular-solid interfaces of the type studied herein in acoustic non-reciprocity applications. Indeed, in this work we only considered direct shock excitation of the 2D granular medium, but not a similar excitation of the plate. It would be of interest to study the non-reciprocal acoustic features of these granular-plate systems, especially given their strong nonlinearity and high asymmetry; this, for example, could yield new types of nonlinear "acoustic diodes" that would support mainly unidirectional wave transmission. Some promising results in this area have already been reported with nonlinear asymmetric lattice systems [64]. A final note concerns the passive self-adaptiveness (or tunability) of the granular-solid interfaces considered to the applied shock excitation. As shown in this work, the nonlinear acoustics of these systems depend on the intensity of the applied shock (or energy), but also on its frequency and wavenumber content (this particular aspect was not studied here, since only uniformly distributed, idealized shocks were considered). The source of this very interesting passive tunability feature could be exploited in the design granular-based protective systems against shock, with the capacity to self-tune their acoustics depending on the type of the applied excitation (e.g., low/high rate, low/high intensity, spatially extended/localized, etc.). This could lead to a new class of passive shock mitigators of enhanced performance.

Appendix 1: The computational algorithm and its numerical stability

The computational algorithm is outlined in the flow chart of Fig. 13.

An iterative scheme computes the converged global interaction force vector $\boldsymbol{F}^{C}_{s+1}$ between the granular medium and

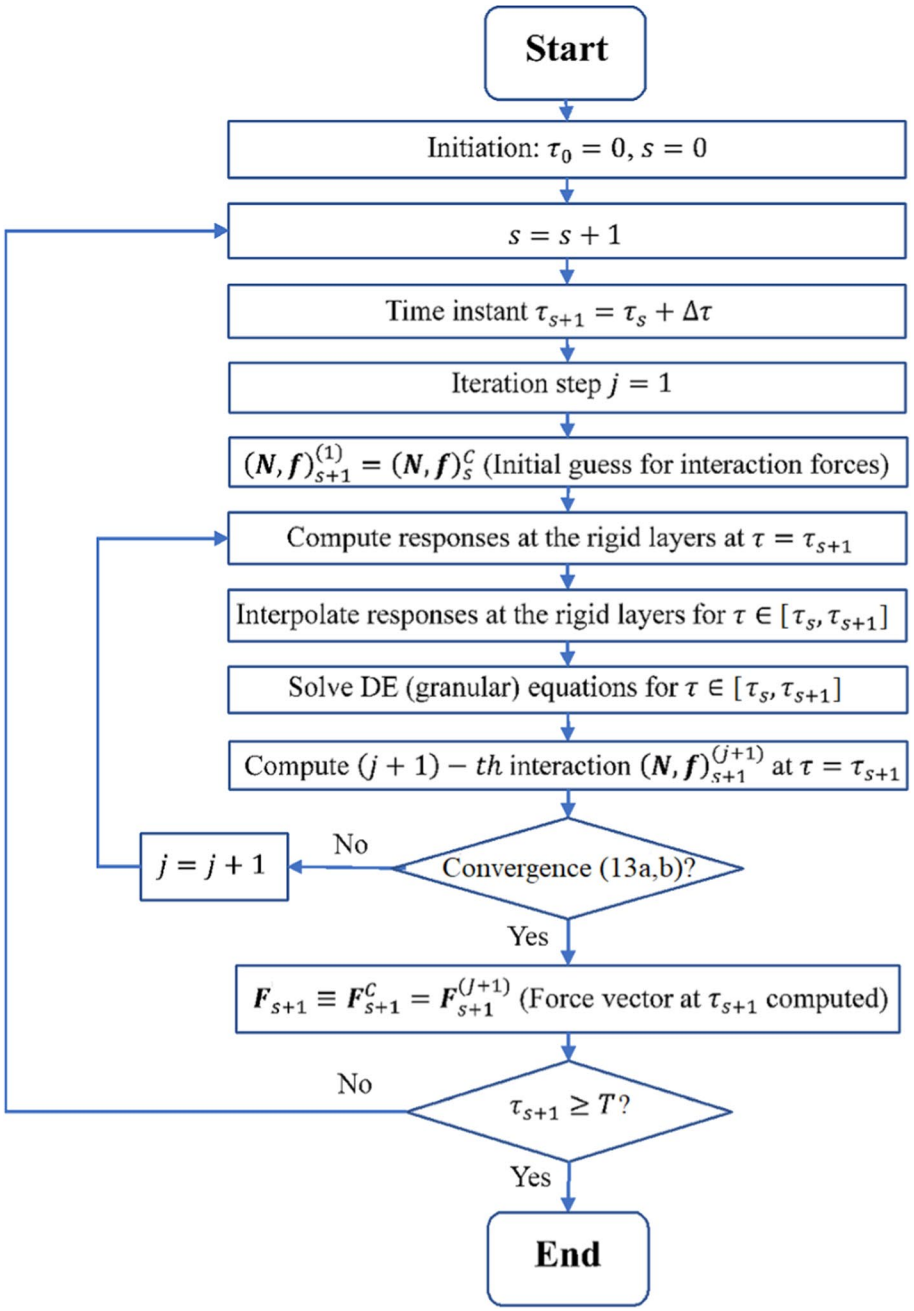

Fig. 13 Flow chart of the computational algorithm for computing the converged interaction forces applied to the plate in the time interval $0 \leq \tau \leq T$; $(\boldsymbol{N},\boldsymbol{f})_{s+1}^{(j)}$ denotes the j-th iteration of the interaction force vector, and $\boldsymbol{F}_{s+1}$ the converged force vector at the time instant τ_{s+1}

the plate at the time instant $\tau = \tau_{s+1}$ once the solution at the previous time instant $\tau = \tau_s$ has been determined (where the notation of the main text holds throughout). The iteration scheme is divided into two distinct phases. In the first phase we consider exclusively the response of the thin plate. To compute the response of the plate in the first iteration ($j = 1$) of the flow chart of Fig. 13 at time instant τ_{s+1}, we select the global force vector applied to the plate as $\boldsymbol{F}_{s+1}^{(1)} = \boldsymbol{F}_s^C$. Then, the first iteration of the response of the plate $\boldsymbol{x}_{s+1}^{(1)}$ at the time instant τ_{s+1}, is computed by solving Eq. (11) using the β-Newmark method based on the assumption of constant acceleration between successive time steps,

$$\dot{\boldsymbol{x}}_{s+1}^{(1)} = \dot{\boldsymbol{x}}_s^C + \left[(1-\gamma)\ddot{\boldsymbol{x}}_s^C + \gamma\ddot{\boldsymbol{x}}_{s+1}^{(1)}\right]\Delta\tau \tag{15a}$$

$$\boldsymbol{x}_{s+1}^{(1)} = \boldsymbol{x}_s^C + \dot{\boldsymbol{x}}_s^C\Delta\tau + \left[\frac{1-2\beta}{2}\ddot{\boldsymbol{x}}_s^C + \beta\ddot{\boldsymbol{x}}_{s+1}^{(1)}\right]\Delta\tau^2 \tag{15b}$$

$$\boldsymbol{M}\ddot{\boldsymbol{x}}_{s+1}^{(1)} + \boldsymbol{K}\boldsymbol{x}_{s+1}^{(1)} = \boldsymbol{F}_{s+1}^{(1)} \tag{15c}$$

with $\beta = 1/4$ and $\gamma = 1/2$. Note that we use the converged values for the response variables at the previous time step τ_s, and that the equations above are linear with respect to the

response "status" vectors of the plate, $\boldsymbol{x}_{s+1}^{(1)}$, $\dot{\boldsymbol{x}}_{s+1}^{(1)}$ and $\ddot{\boldsymbol{x}}_{s+1}^{(1)}$, at the current time instant τ_{s+1}. Once the first iteration for the status vectors $\boldsymbol{x}_{s}^{(1)}$, $\dot{\boldsymbol{x}}_{s}^{(1)}$ and $\boldsymbol{x}_{s+1}^{(1)}$ have been evaluated, the first iteration of the displacement vector $\boldsymbol{x}^{(1)}(\tau)$ of the plate can be evaluated over the entire time interval $\tau \in [\tau_s, \tau_{s+1}]$ as follows:

$$\boldsymbol{x}^{(1)}(\tau) = \boldsymbol{x}_s^C + (\tau - \tau_s)\dot{\boldsymbol{x}}_s^C + \frac{(\tau-\tau_s)^2}{\Delta\tau^2}\left(\boldsymbol{x}_{s+1}^{(1)} - \boldsymbol{x}_s^C - \dot{\boldsymbol{x}}_s^C\Delta\tau\right) \tag{16}$$

This expression is based on the assumption of (approximately) constant acceleration between successive time steps. Once the response of the thin plate in the entire interval $\tau \in [\tau_s, \tau_{s+1}]$ is determined, the responses of the rigid layers at the free boundary of the plate are also available, which act as a moving boundary for the DE system modeling the granular medium. This completes the first phase of the first iteration, as it evaluates the first iterate of the plate response.

In the second phase of the first iteration (i.e., still for $j = 1$), we compute the response of the granular medium at the time instant τ_{s+1}. To this end, the DE Eqs (1) are solved numerically using the fourth order Runge–Kutta method. To this end, the DE system (1) is transformed into a set of first-order differential equations,

$$\dot{\boldsymbol{u}}_b^{(1)} = \boldsymbol{v}_b^{(1)} \tag{17a}$$

$$\dot{\boldsymbol{v}}_b^{(1)} = \boldsymbol{L}\left(\boldsymbol{u}_b^{(1)}, \boldsymbol{v}_b^{(1)}, \boldsymbol{x}^{(1)}(\tau), \dot{\boldsymbol{x}}^{(1)}(\tau)\right) \tag{17b}$$

or,

$$\dot{\boldsymbol{w}}_b^{(1)} = \boldsymbol{G}\left(\boldsymbol{w}_b^{(1)}, \boldsymbol{x}^{(1)}(\tau), \dot{\boldsymbol{x}}^{(1)}(\tau)\right), \quad \tau \in [\tau_s, \tau_{s+1}] \tag{17c}$$

where $\boldsymbol{u}_b^{(1)}$ denotes the first iteration of the displacement vector of all granules in the time interval $\tau \in [\tau_s, \tau_{s+1}]$, $\boldsymbol{v}_b^{(1)} = \dot{\boldsymbol{u}}_b^{(1)}$, $\boldsymbol{w}_b^{(1)} \equiv \left(\boldsymbol{u}_b^{(1)}, \boldsymbol{v}_b^{(1)}\right)$, and $\boldsymbol{L}(\cdot), \boldsymbol{G}(\cdot)$ are highly discontinuous functions, given that the interaction forces between granules can be Hertzian, frictional and viscous (due to structural damping of the material of the granules). The DE system (17c) is then numerically solved by applying the fourth order Runge–Kutta method,

This computation yields the status vectors of the first iteration of the granular medium at $\tau = \tau_{s+1}$. Following that, the second iteration of the interaction forces at τ_{s+1} is computed by applying Eqs (2) and (5) with the first iteration of the plate and granular mediums responses. Hence, we compute the second iterates of the interaction force vectors applied to the plate, namely, $\boldsymbol{F}_{s+1}^{(2)} \equiv \left(\boldsymbol{N}_{s+1}^{(2)}, \boldsymbol{f}_{s+1}^{(2)}\right)$ at time instant τ_{s+1}. This competes the second phase of the first iteration at τ_{s+1}. Then, the previous iteration scheme can continue with the second iteration at τ_{s+1}, setting $j = 2$, and repeating the two previous phases, and so on.

This iterative scheme generates a nonlinear map that relates the j-th iterates of the interaction forces at the rigid layers on the plate to the $(j+1)$-th iterates, or in symbolic form, $\left[\boldsymbol{N}_{s+1}^{(j)}, \boldsymbol{f}_{s+1}^{(j)}\right] \rightarrow \left[\boldsymbol{N}_{s+1}^{(j+1)}, \boldsymbol{f}_{s+1}^{(j+1)}\right]$ at the current time step τ_{s+1}. With increasing number of iterations the interaction forces are expected to converge (the conditions for convergence are discussed below), by satisfying the following two convergence criteria,

$$\left|f_{k,s+1}^{(j+1)} - f_{k,s+1}^{(j)}\right| < abstol; \left|N_{k,s+1}^{(j+1)} - N_{k,s+1}^{(j)}\right| < abstol \tag{18a}$$

$$\left|f_{k,s+1}^{(j+1)} - f_{k,s+1}^{(j)}\right| / \left|f_{k,s+1}^{(j)}\right| < reltol; \left|N_{k,s+1}^{(j+1)} - N_{k,s+1}^{(j)}\right| / N_{k,s+1}^{(j)} < reltol \tag{18b}$$

where *abstol* denotes the absolute tolerance, and *reltol* the relative tolerance. As a reminder, $N_{k,s+1}^{(j)}$ and $f_{k,s+1}^{(j)}$ denote the k-th elements of the global normal and tangential interaction force vectors on the plate, $\boldsymbol{N}_{s+1}^{(j)}$ and $\boldsymbol{f}_{s+1}^{(j)}$ at time instant τ_{s+1}. The interaction force vectors are considered to have converged if either (18a) and/or (18b) is satisfied for all nodes k at the rigid layers of the plate (cf. Fig. 3). Supposing that convergence has been achieved at the J-th iteration, we denote the converged interaction force vectors at time instant τ_{s+1} by $\left(\boldsymbol{N}_{s+1}^{C}, \boldsymbol{f}_{s+1}^{C}\right) \equiv \left(\boldsymbol{N}_{s+1}^{(J)}, \boldsymbol{f}_{s+1}^{(J)}\right)$. Once the interaction forces on the plate have converged, all the response status vectors at the current time step τ_{s+1} will have converged as well, and the computation proceeds to the next time step τ_{s+2}, where the outlined iteration scheme is repeated until the entire time interval T of the simulation is exhausted.

Clearly, central to the stability and convergence of the computational algorithm is the stability of the previous global map $\left[\boldsymbol{N}_{s+1}^{(j)}, \boldsymbol{f}_{s+1}^{(j)}\right] \rightarrow \left[\boldsymbol{N}_{s+1}^{(j+1)}, \boldsymbol{f}_{s+1}^{(j+1)}\right]$ at an arbitrary—say the $(j+1)$th iteration. To ensure the convergence of the β -Newmark method, the time step increment $\Delta\tau$ should be sufficiently small so that variations of the interaction forces due to the time delay of the wave propagation at a contact point at τ_{s+1} has negligible effects on the responses at the other contact points at the current time step τ_{s+1}. Hence, since the interaction forces at a contact point of the plate have an approximately local effect, the next iteration of the interaction forces at that contact point should also be determined only by the local response at the contact point (i.e., we assume that $\Delta\tau$ is small enough so that "coupling" effects between different contact points may be neglected). Accordingly, the global map $\left[\boldsymbol{N}_{s+1}^{(j)}, \boldsymbol{f}_{s+1}^{(j)}\right] \rightarrow \left[\boldsymbol{N}_{s+1}^{(j+1)}, \boldsymbol{f}_{s+1}^{(j+1)}\right]$ can be decomposed into individual 2D local maps $\left(N_{k,s+1}^{(j)}, f_{k,s+1}^{(j)}\right) \rightarrow \left(N_{k,s+1}^{(j+1)}, f_{k,s+1}^{(j+1)}\right)$ at each contact point k at the current time step. Clearly, *the global map is stable if all 2D local maps are stable* (i.e., for every contact point k on the plate).

Note that the $(j+1)$th iterate of each interaction force component at the contact point k of the plate at time instant τ_{s+1} can be expressed in explicit form as follows,

$$N_{k,s+1}^{(j+1)} = -\frac{4}{3}E^*\sqrt{R^*}\left[u_{k,p,n,s+1}^{(j)} - u_{k,b,n,s+1}^{(j)}\right]_+^{3/2} \tag{19a}$$

$$f_{k,s+1}^{(j+1)} = -\mu\left|N_{k,s+1}^{(j+1)}\right| \tanh\left[k_s\left(v_{k,p,t,s+1}^{(j)} - v_{k,b,t,s+1}^{(j)}\right)\right] \tag{19b}$$

where referring to the notation introduced in Fig. 3, the subscripts p, b denote plate and contacting granule, respectively, whereas the subscripts n, t denote normal and tangential components, respectively. Hence, in (19a,b) the variables $u_{k,p,n,s+1}^{(j)}$ and $u_{k,b,n,s+1}^{(j)}$ $\left(u_{k,p,t,s+1}^{(j)}\right.$ and $\left.u_{k,b,t,s+1}^{(j)}\right)$ denote the j-th iterates of the normal (tangential) components of the deformations of the plate and the contacting granule at time instant τ_{s+1}, respectively. In addition, $v = \dot{u}$, represents the corresponding velocity. Furthermore, $N_{k,s+1}^{(j+1)}$ and $f_{k,s+1}^{(j+1)}$ denote the normal and tangential forces applied at the kj-th contact point of the plate at the current time instant τ_{s+1}. As the small rigid layers at the boundary of the plate are assumed to be flat and massless, the dissipative term in the normal force is omitted, while $E^* = E_b/\left(1-\nu_b^2\right)$ and $R^* = R_b$.

Relations (19a, b) are in scalar form, with the positive directions defined in Fig. 3. To evaluate the stability of the 2D local map $\left(N_{k,s+1}^{(j)}, f_{k,s+1}^{(j)}\right) \rightarrow \left(N_{k,s+1}^{(j+1)}, f_{k,s+1}^{(j+1)}\right)$ it is necessary to examine its (2×2) Jacobian matrix,

$$\frac{\partial\left(N_{k,s+1}^{(j+1)}, f_{k,s+1}^{(j+1)}\right)}{\partial\left(N_{k,s+1}^{(j)}, f_{k,s+1}^{(j)}\right)} = \frac{\partial\left(N_{k,s+1}^{(j+1)}, f_{k,s+1}^{(j+1)}\right)}{\partial\left(u_{k,p,n,s+1}^{(j)} - u_{k,b,n,s+1}^{(j)}, v_{k,p,t,s+1}^{(j)} - v_{k,b,t,s+1}^{(j)}\right)}\left[\frac{\partial\left(N_{k,s+1}^{(j+1)}, f_{k,s+1}^{(j+1)}\right)}{\partial\left(u_{k,p,n,s+1}^{(j)} - u_{k,b,n,s+1}^{(j)}, v_{k,p,t,s+1}^{(j)} - v_{k,b,t,s+1}^{(j)}\right)}\right] \tag{20}$$

and compute its eigenvalues. The first multiplicative term in (20) can be explicitly evaluated by relations (19a, b). To evaluate the second multiplicative term, we consider the discretized differential equations at successive time steps to evaluate the sensitivities of the responses of the plate and granules at the current time step. The response of the plate at the j-th iteration and time instant τ_{s+1} subject to the interaction forces at the same iteration can be computed by solving Eq. (11):

$$\dot{\boldsymbol{x}}_{s+1}^{(j)} = \dot{\boldsymbol{x}}_s^C + \frac{1}{2}\ddot{\boldsymbol{x}}_s^C\Delta\tau + \frac{1}{2}\ddot{\boldsymbol{x}}_{s+1}^{(j)}\Delta\tau \tag{21a}$$

$$\boldsymbol{x}_{s+1}^{(j)} = \boldsymbol{x}_s^C + \dot{\boldsymbol{x}}_s^C\Delta\tau + \frac{1}{4}\ddot{\boldsymbol{x}}_s^C\Delta\tau^2 + \frac{1}{4}\ddot{\boldsymbol{x}}_{s+1}^{(j)}\Delta\tau^2 \tag{21b}$$

$$\ddot{\boldsymbol{x}}_{s+1}^{(j)} = \left(\boldsymbol{M} + \frac{1}{4}\boldsymbol{K}\Delta\tau^2\right)^{-1}\boldsymbol{F}_{s+1}^{(j)} - \left(\boldsymbol{M} + \frac{1}{4}\boldsymbol{K}\Delta\tau^2\right)^{-1}\boldsymbol{K}\left(\boldsymbol{x}_s^C + \dot{\boldsymbol{x}}_s^C\Delta\tau + \frac{1}{4}\ddot{\boldsymbol{x}}_s^C\Delta\tau^2\right) \tag{21c}$$

We note at this point that the normal and tangential displacements at the $k-th$ contact point can be linearly related to the plate displacement vector $\boldsymbol{x}_{s+1}^{(j)}$ as follows:

$$u_{k,p,n,s+1}^{(j)} = \boldsymbol{T}_{k,n}\boldsymbol{x}_{s+1}^{(j)} \tag{22a}$$

$$u_{k,p,t,s+1}^{(j)} = \boldsymbol{T}_{k,t}\boldsymbol{x}_{s+1}^{(j)} \tag{22b}$$

$$\boldsymbol{T}_k = \left(\boldsymbol{T}_{k,n}, \boldsymbol{T}_{k,t}\right)^T \tag{22c}$$

Note that $u_{k,p,n,s+1}^{(j)}$ and $u_{k,p,t,s+1}^{(j)}$ are the components of $\boldsymbol{x}_{s+1}^{(j)}$ at the normal and tangential DOFs at the node of the k-th contact point, respectively; also, $\boldsymbol{T}_{k,n}$ and $\boldsymbol{T}_{k,t}$ are sparse vectors whose only non-zero terms, with value equal to unity, are located at the normal and tangential driving DOFs, respectively, for the k-th contact point. Since the corresponding components of the force vector $\boldsymbol{F}_{s+1}^{(j)}$ are $N_{k,s+1}^{(j)}$ and $f_{k,s+1}^{(j)}$, It follows that:

$$\frac{\partial \boldsymbol{F}_{s+1}^{(j)}}{\partial\left(N_{k,s+1}^{(j)}, f_{k,s+1}^{(j)}\right)} = \boldsymbol{T}_k^T \tag{23}$$

Therefore, the plate component of the second multiplicative term in Eq. (20) could be computed by the chain rule:

$$\frac{\partial\left(u_{k,p,n,s+1}^{(j)}, u_{k,p,t,s+1}^{(j)}\right)}{\left(N_{k,s+1}^{(j)}, f_{k,s+1}^{(j)}\right)} = \frac{\partial\left(u_{k,p,n,s+1}^{(j)}, u_{k,p,t,s+1}^{(j)}\right)}{\partial \boldsymbol{x}_{s+1}^{(j)}} \cdot \frac{\partial \boldsymbol{x}_{s+1}^{(j)}}{\partial \ddot{\boldsymbol{x}}_{s+1}^{(j)}} \cdot \frac{\partial \ddot{\boldsymbol{x}}_{s+1}^{(j)}}{\partial \boldsymbol{F}_{s+1}^{(j)}} \cdot \frac{\partial \boldsymbol{F}_{s+1}^{(j)}}{\partial\left(N_{k,s+1}^{(j)}, f_{k,s+1}^{(j)}\right)} \tag{24a}$$

$$\frac{\partial\left(v_{k,p,n,s+1}^{(j)}, v_{k,p,t,s+1}^{(j)}\right)}{\partial\left(N_{k,s+1}^{(j)}, f_{k,s+1}^{(j)}\right)} = \frac{\partial\left(\dot{u}_{k,p,n,s+1}^{(j)}, \dot{u}_{k,p,t,s+1}^{(j)}\right)}{\partial \dot{\boldsymbol{x}}_{s+1}^{(j)}} \cdot \frac{\partial \dot{\boldsymbol{x}}_{s+1}^{(j)}}{\partial \ddot{\boldsymbol{x}}_{s+1}^{(j)}} \cdot \frac{\partial \ddot{\boldsymbol{x}}_{s+1}^{(j)}}{\partial \boldsymbol{F}_{s+1}^{(j)}} \cdot \frac{\partial \boldsymbol{F}_{s+1}^{(j)}}{\partial\left(N_{k,s+1}^{(j)}, f_{k,s+1}^{(j)}\right)} \tag{24b}$$

Substituting relations (21), (22) and (23) into Eqs. (24a, b), we derive the following expressions:

$$\frac{\partial\left(u^{(j)}_{k,p,n,s+1},u^{(j)}_{k,p,t,s+1}\right)}{\partial\left(N^{(j)}_{k,s+1},f^{(j)}_{k,s+1}\right)}=\frac{1}{4}\Delta\tau^2\boldsymbol{T}_k\left(\boldsymbol{M}+\frac{1}{4}\boldsymbol{K}\Delta\tau^2\right)^{-1}\boldsymbol{T}_k^T \tag{25a}$$

$$\frac{\partial\left(v^{(j)}_{k,p,n,s+1},v^{(j)}_{k,p,t,s+1}\right)}{\partial\left(N^{(j)}_{k,s+1},f^{(j)}_{k,s+1}\right)}=\frac{1}{2}\Delta\tau\boldsymbol{T}_k\left(\boldsymbol{M}+\frac{1}{4}\boldsymbol{K}\Delta\tau^2\right)^{-1}\boldsymbol{T}_k^T \tag{25b}$$

Since we assumed that the effect of the interaction forces is nearly local, it is logical to assume that due to the symmetry of the rigid layers the normal forces cannot generate tangential responses, while the tangential forces cannot generate normal responses at the current time step. This yields the following further approximations:

$$\frac{\partial u^{(j)}_{k,p,n,s+1}}{\partial f^{(j)}_{k,s+1}}\approx\frac{\partial v^{(j)}_{k,p,n,s+1}}{\partial f^{(j)}_{k,s+1}}\approx\frac{\partial u^{(j)}_{k,p,t,s+1}}{\partial N^{(j)}_{k,s+1}}\approx\frac{\partial v^{(j)}_{k,p,t,s+1}}{\partial N^{(j)}_{k,s+1}}\approx 0 \tag{26}$$

Substituting (26) to relations (25a, b), we derive the following closed form simplified diagonalized sensitivity matrix for the responses at the contact points on the plate:

$$\frac{\partial\left(u^{(j)}_{k,p,n,s+1},v^{(j)}_{k,p,t,s+1}\right)}{\partial\left(N^{(j)}_{k,s+1},f^{(j)}_{k,s+1}\right)}=Diag\left[\frac{1}{4}\Delta\tau^2\boldsymbol{T}_{k,n}\left(\boldsymbol{M}+\frac{1}{4}\boldsymbol{K}\Delta\tau^2\right)^{-1}\boldsymbol{T}_{k,n}^T,\frac{1}{2}\Delta\tau\boldsymbol{T}_{k,t}\left(\boldsymbol{M}+\frac{1}{4}\boldsymbol{K}\Delta\tau^2\right)^{-1}\boldsymbol{T}_{k,t}^T\right] \tag{27}$$

Similarly, by imposing the previous assumptions we can compute the corresponding sensitivities $\frac{\partial\left(u^{(j)}_{k,b,n,s+1},v^{(j)}_{k,b,t,s+1}\right)}{\partial\left(N^{(j)}_{k,s+1}f^{(j)}_{k,s+1}\right)}$ of the contacting boundary granules. However, as the mass of a single granule is much larger than the mass of the finite element of the plate attached to the contacting rigid layer, it is logical to assume that the response of the rigid layer should be much more sensitive with respect to the interaction forces compared to the response of the granule. Hence, as an additional approximation, we may neglect the sensitivities related to the granule responses, thus simplifying Eq. (20) as follows:

$$\frac{\partial\left(N^{(j+1)}_{k,s+1},f^{(j+1)}_{k,s+1}\right)}{\partial\left(N^{(j)}_{k,s+1},f^{(j)}_{k,s+1}\right)}\approx\frac{\partial\left(N^{(j+1)}_{k,s+1},f^{(j+1)}_{k,s+1}\right)}{\partial\left(u^{(j)}_{k,p,n,s+1},v^{(j)}_{k,p,t,s+1}\right)}\cdot\frac{\partial\left(u^{(j)}_{k,p,n,s+1},v^{(j)}_{k,p,t,s+1}\right)}{\partial\left(N^{(j)}_{k,s+1},f^{(j)}_{k,s+1}\right)} \tag{28}$$

As a final step, the Jacobian matrix of the local nonlinear map at contact point k on the rigid layer of the plate, $\left(N^{(j)}_{k,s+1},f^{(j)}_{k,s+1}\right)\rightarrow\left(N^{(j+1)}_{k,s+1},f^{(j+1)}_{k,s+1}\right)$ is approximated in closed form by substituting the relations (19a, b) and (27) into (28).

As the Jacobian matrix is semi-negative definite for arbitrary interaction forces, according to the Banach fixed point theorem the local map has a unique fixed point (i.e., it is guaranteed to converge to a solution), and its eigenvalues are approximately evaluated in closed form as follows:

$$\lambda_{k1,s+1}=-\frac{1}{2}E^*\sqrt{R^*}\Delta\tau^2\boldsymbol{T}_{k,n}\left(\boldsymbol{M}+\frac{1}{4}\boldsymbol{K}\Delta\tau^2\right)^{-1}\boldsymbol{T}_{k,n}^T\left(u^{(j)}_{k,p,n,s+1}-u^{(j)}_{k,b,n,s+1}\right)_+^{1/2} \tag{29a}$$

$$-\frac{1}{2}\mu k_s\left|N^{(j)}_{k,s+1}\right|\left|\Delta\tau T_{k,t}\left(\boldsymbol{M}+\frac{1}{4}\boldsymbol{K}\Delta\tau^2\right)^{-1}\boldsymbol{T}_{k,t}^T\cosh\left[k_s\left(v^{(j)}_{k,p,t,s+1}-v^{(j)}_{k,b,t,s+1}\right)\right]^{-2}\right| \tag{29b}$$

Accordingly, the local map is stable if the moduli of both eigenvalues are smaller than unity, which gives the conditions (27a, b).

Appendix 2

Below we provide links for the following animations for the acoustics of:

The monolithic plate of Fig. 11a subject to a uniform impulse of 1 μs and 20000 N/m intensity https://uofi.box.com/s/13ia09hrmnsctw2tl5xm47p6te78qzby

The granular-solid interface of Fig. 11c with uniform initial velocities $v_0 = 0.3414$ m/s of its five left granules, corresponding to the same energy input to case (i) for the monolithic plate https://uofi.box.com/s/tvxsuqehqfhgs1w8ype4s89tcwve0qly

The granular-solid interface of Fig. 11c with uniform initial velocities $v_0 = 0.5$ m/s and $v_0 = 1.0$ m/s of its five left granules https://uofi.box.com/s/xi8hp6zzz61ofanvy6iq102t8e00h9lv, https://uofi.box.com/s/5ck6xjbnhac76t6bf0d044zdwikgxot2

Acknowledgements This work was supported in part by the China Scholarship Council (Grant 201706160084) that supported the visit of Qifan Zhang to the University of Illinois, Urbana Champaign.

Compliance with Ethical Standards

Conflict of interest The authors declare that they have no conflict of interest.

References

1. Lazaridi, A.N., Nesterenko, V.F.: Observation of a new type of solitary waves in a one-dimensional granular medium. J. Appl. Mech. Tech. Phys. **26**(3), 405–408 (1985)
2. Nesterenko, V.F.: Propagation of nonlinear compression pulses in granular media. J. Appl. Mech. Tech. Phys. **24**, 733–743 (1983)
3. Nesterenko, V.F.: Solitary waves in discrete media with anomalous compressibility and similar to "sonic vacuum." J. Phys. IV **4**(C8), 729–734 (1994)
4. Nesterenko, V.F.: Dynamics of Heterogeneous Materials. Springer, New York (2001)
5. Daraio, C., Nesterenko, V.F., Herbold, E.B., Jin, S.: Strongly nonlinear waves in a chain of Teflon beads. Phys. Rev. E **72**, 016603 (2005)
6. Starosvetsky, Y., Jayaprakash, K.R., Hasan, M.A., Vakakis, A.F.: Topics on the Nonlinear Dynamics and Acoustics of Ordered Granular Media. World Scientific Press, Singapore (2017)
7. Hasan, M.A., Cho, S., Remick, K., McFarland, D.M., Vakakis, A.F., Kriven, W.M.: Experimental study of nonlinear acoustic bands and propagating breathers in ordered granular media embedded in matrix. Granul. Matter **17**, 49–72 (2015)
8. Starosvetsky, Y., Vakakis, A.F.: Traveling waves and localized modes in one-dimensional homogeneous granular chains with no pre-compression. Phys. Rev. E **82**(2), 026603 (2010)
9. Zhang, Z., Manevitch, L.I., Smirnov, V., Bergman, L.A., Vakakis, A.F.: Extreme nonlinear energy exchanges in a geometrically nonlinear lattice oscillating in the plane. J. Mech. Phys. Solids **110**, 1–20 (2018)
10. Hasan, M.A., Starosvetsky, Y., Vakakis, A.F., Manevitch, L.I.: Nonlinear targeted energy transfer and macroscopic analogue of the quantum Landau-Zener effect in coupled granular chains. Physica D **252**, 46–58 (2013)
11. Zhang, Z., Koroleva, I., Manevitch, L.I., Bergman, L.A., Vakakis, A.F.: Non-reciprocal acoustics and dynamics in the in-plane oscillations of a geometrically nonlinear lattice. Phys. Rev. E **94**(3), 032214 (2016)
12. Zhang, Q., Li, W., Lambros, J., Bergman, L.A., Vakakis, A.F.: Pulse transmission and acoustic non-reciprocity in a granular channel with symmetry-breaking clearances. Granul. Matter **22**(1), 20 (2020)
13. Cui, J., Yang, T., Chen, L.: Frequency-preserved non-reciprocal acoustic propagation in a granular chain. Appl. Phys. Lett. **112**, 181904 (2018)
14. Melo, F., Job, S., Santibanez, F., Tapia, F.: Experimental evidence of shock mitigation in a Hertzian tapered chain. Phys. Rev. E **73**(4), 041305 (2006)
15. Hong, J.: Universal power-law decay of the impulse energy in granular protectors. Phys. Rev. Lett. **94**, 108001 (2005)
16. Sen, S., Manciu, F.S., Manciu, M.: Thermalizing an impulse. Phys. A **299**, 551–558 (2001)
17. Sen, S., Mohan, T.R.K., Visco, D.P., Swaminathan, S., Sokolow, A., Avalos, A., Nakagawa, M.: Using mechanical energy as a probe for the detection and imaging of shallow buried inclusions in dry granular beds. Int. J. Mod. Phys. B **19**, 2951–2973 (2005)
18. Spadoni, A., Daraio, C.: Generation and control of sound bullets with a nonlinear acoustic lens. Proc. Natl. Acad. Sci. **107**(16), 7230–7234 (2010)
19. Donahue, C.M., Anzel, P.W.J., Bonanomi, L., Keller, T.A., Daraio, C.: Experimental realization of a nonlinear acoustic lens with a tunable focus. Appl. Phys. Lett. **104**(1), 014103 (2014)
20. Lawney, B.P., Luding, S.: Frequency filtering in disordered granular chains. Acta Mech. **225**, 2385–2407 (2014)
21. Li, F., Anzel, P., Yang, J., Kevrekidis, P.G., Daraio, C.: Granular acoustic switches and logic elements. Nat. Commun. **5**, 5311 (2014)
22. Job, S., Melo, F., Sokolow, A., Sen, S.: How Hertzian solitary waves interact with boundaries in a 1D granular medium. Phys. Rev. Lett. **94**, 178002 (2005)
23. Yang, J., Silvestro, C., Khatri, D., Nardo, L.D., Daraio, C.: Interaction of highly nonlinear solitary waves with linear elastic media. Phys. Rev. E **83**, 046606 (2011)
24. Yang, J., Khatri, D., Anzel, P., Daraio, C.: Interaction of highly nonlinear solitary waves with thin plates. Int. J. Solids Struct. **49**, 1463–1471 (2012)
25. Potekin, R., McFarland, D.M., Vakakis, A.F.: Nonlinear wave scattering at the flexible interface of a granular dimer chain. Granul. Matter **15**, 51–68 (2016)
26. Zhang, Q., Potekin, R., Li, W., Vakakis, A.F.: Nonlinear wave scattering at the interface of granular dimer chains and an elastically supported membrane. Int. J. Solids Struct. **182–183**(202001), 46–63 (2020)
27. Awasthi, A.P., Smith, K.J., Geubelle, P.H., Lambros, J.: Propagation of solitary waves in 2D granular media: a numerical study. Mech. Mater. **54**, 100–112 (2012)
28. Leonard, A., Daraio, C.: Stress wave anisotropy in centered square highly nonlinear granular systems. Phys. Rev. Lett. **108**, 214301 (2012)
29. Leonard, A., Ponson, L., Daraio, C.: Wave mitigation in ordered networks of granular chains. J. Mech. Phys. Solids **73**, 103–117 (2014)
30. Leonard, A., Chong, C., Kevrekidis, P.G., Daraio, C.: Traveling waves in 2D hexagonal granular crystal lattices. Granul. Matter. **16**, 531–542 (2014)
31. Manjunath, M., Awasthi, A.P., Geubelle, P.H.: Plane wave propagation in 2D and 3D monodisperse periodic granular media. Granul. Matter **16**, 141–150 (2014)
32. Manjunath, M., Awasthi, A.P., Geubelle, P.H.: Wave propagation in 2D random granular media. Physica D **266**, 42–48 (2014)
33. Szelengowicz, I., Kevrekidis, P.G., Daraio, C.: Wave propagation in square granular crystals with spherical interstitial intruders. Phys. Rev. E **86**, 061306 (2012)
34. Szelengowicz, I., Hasan, M.A., Starosvetsky, Y., Vakakis, A.F., Daraio, C.: Energy equipartition in two-dimensional granular systems with spherical intruders. Phys. Rev. E **87**, 032204 (2013)
35. Lisyansky, A., Meimukhin, D., Starosvetsky, Y.: Primary wave transmission in the hexagonally packed, damped granular crystal with a spatially varying cross section. Commun. Nonlinear Sci. Numer. Simul. **27**(1–3), 193–205 (2015)
36. Szelengowicz, I. M. N., Analysis and optimization of stress wave propagation in 2D granular crystals with defects, Ph.D. Thesis., California Institute of Technology (2013)
37. Bassett, D.S., Owens, E.T., Porter, M.A., Manning, M.L., Daniels, K.E.: Extraction of force-chain network architecture in granular materials using community detection. Soft Matter **11**(14), 2731–2744 (2015)
38. Berthier, E., Porter, M.A., Daniels, K.E.: Forecasting failure locations in 2D disordered lattices. Proc. Natl. Acad. Sci. **116**(34), 16742–16749 (2019)
39. Bassett, D.S., Owens, E.T., Daniels, K.E., Porter, M.A.: Influence of network topology on sound propagation in granular materials. Phys. Rev. E **86**(4), 041306 (2018)
40. Xu, J., Zheng, B.: Stress wave propagation in 2D buckyball lattice. Sci. Rep. **6**(1), 1–8 (2016)
41. Wang, J., Chu, X., Zhang, J., Liu, H.: The effects of microstructure on wave velocity and wavefront in granular assemblies with binary-sized particles. Int. J. Solids Struct. **159**, 156–162 (2019)

42. Hua, T., Van Gorder, R.A.: Wave propagation and pattern formation in 2D hexagonally-packed granular crystals under various configurations. Granul. Matter **21**, 3 (2019)
43. Li, L., Yang, X., Zhang, W.: Two interactional solitary waves propagating in two-dimensional hexagonal packing granular system. Granul. Matter **20**, 49 (2018)
44. Starosvetsky, Y., Hasan, M.A., Vakakis, A.F.: "Nonlinear pulse equipartition in weakly coupled ordered granular chains with no pre-compression. J. Comp. Nonlinear Dyn. **8**, 034504 (2013)
45. Zhang, Y., Hasan, M.A., Starosvetsky, Y., McFarland, D.M., Vakakis, A.F.: Nonlinear mixed solitary—shear waves and pulse equi-partition in a granular network. Physica D **291**, 45–61 (2015)
46. Starosvetsky, Y., Hasan, M.A., Vakakis, A.F., Manevitch, L.I.: Strongly nonlinear beat phenomena and energy exchanges in weakly coupled granular chains on elastic foundations. SIAM J. Appl. Math. **72**(1), 337–361 (2012)
47. Hasan, M.A., Cho, S., Remick, K., Vakakis, A.F., McFarland, D.M., Kriven, W.K.: Primary pulse transmission in coupled steel granular chains embedded in PDMS matrix: experiment and modeling. Int. J. Solids Struct. **50**, 3207–3224 (2013)
48. Ben-Meir, Y., Starosvetsky, Y.: Modulation of solitary waves and formation of stable attractors in granular scalar models subjected to on-site perturbation. Wave Motion **51**, 685–715 (2014)
49. Yang, J., Sutton, M.: Nonlinear wave propagation in a hexagonally packed granular channel under rotational dynamics. Int. J. Solids. Struct. **77**(3), 65–73 (2015)
50. Goldenberg, C., Goldhirsch, I.: Friction enhances elasticity in granular solids. Nature **435**, 188–191 (2005)
51. Chattoraj, J., Gendelman, O., Ciamarra, M.P., Procaccia, I.: Oscillatory instabilities in frictional granular matter. Phys. Rev. Lett. **123**, 098003 (2019)
52. Charan H., Gendelman O., Procaccia I., Sheffer Y. Giant Amplification of Small Perturbations in Frictional Amorphous Solid, arXiv:2001.06862 [cond-mat.soft]
53. Tsuji, Y., Tanaka, T., Ishida, T.: Lagrangian numerical simulation of plug flow of cohesionless particles in a horizontal pipe. Powder Technol. **71**, 239–250 (1992)
54. Cundall, P.A., Strack, O.D.: A discrete numerical model for granular assemblies. Géotechnique **29**(1), 47–65 (1979)
55. Adersson, S., Söderberg, A., Björklund, S.: Friction models for sliding dry, boundary and mixed lubricated contacts. Tribol. Int. **40**, 580–587 (2007)
56. Pennestrì, E., Rossi, V., Salvini, P., Valentini, P.P.: Review and comparison of dry friction force models. Nonl. Dyn. **83**, 1785–1801 (2016)
57. Timoshenko, S.P., Goyder, J.N.: Theory of Elasticity, 3rd edn. McGraw Hill, New York (2010)
58. Whitham, G.B.: Linear and Nonlinear Waves. Wiley Interscience, New York (1974)
59. Starosvetsky, Y., Vakakis, A.F.: Primary wave transmission in systems of elastic rods with granular interfaces. Wave Motion **48**(7), 568–585 (2011)
60. Zienkiewicz, O.C., Taylor, R.L., Nithiarasu, P., Zhu, J.Z.: The Finite Element Method. McGraw-Hill, London (1977)
61. Hughes, T.J.R.: The Finite Element Method: Linear Static and Dynamic Finite Element Analysis. Dover Publications, New York (2000)
62. Hasan, M.A., Vakakis, A.F., McFarland, D.M.: Nonlinear localization, passive wave arrest and traveling breathers in two-dimensional granular networks with discontinuous lateral boundary conditions. Wave Motion **60**, 196–219 (2016)
63. Vakakis, A.F., Manevitch, L.I., Mikhlin, Yu.V., Pilipchuk, V.N., Zevin, A.A.: Normal Modes and Localization in Nonlinear Systems. John Wiley & Sons, New York (1996)
64. Mojahed, A., Bunyan, J., Tawfick, S., Vakakis, A.F.: Tunable acoustic non-reciprocity in strongly nonlinear waveguides with asymmetry. Phys. Rev. Appl. **12**, 034033 (2019)